

Estimating Graph Dimension with Cross-validated Eigenvalues

Fan Chen¹, Sébastien Roch², Karl Rohe¹, and Shuqi Yu²

¹Department of Statistics, University of Wisconsin–Madison

²Department of Mathematics, University of Wisconsin–Madison

August 10, 2021

Abstract

In applied multivariate statistics, estimating the number of latent dimensions or the number of clusters is a fundamental and recurring problem. One common diagnostic is the scree plot, which shows the largest eigenvalues of the data matrix in decreasing order; the user searches for a “gap” or “elbow” in the decaying eigenvalues; unfortunately, these patterns can hide beneath the bias of the sample eigenvalues. This methodological problem is conceptually difficult because, in many situations, there is only enough signal to detect a subset of the k population dimensions/eigenvectors. In this situation, one could argue that the correct choice of k is the number of detectable dimensions. We alleviate these problems with *cross-validated eigenvalues*. Under a large class of random graph models, without any parametric assumptions, we provide a p -value for each sample eigenvector. It tests the null hypothesis that this sample eigenvector is orthogonal to (i.e., uncorrelated with) the true latent dimensions. This approach naturally adapts to problems where some dimensions are not statistically detectable. In scenarios where all k dimensions can be estimated, we prove that our procedure consistently estimates k . In simulations and a data example, the proposed estimator compares favorably to alternative approaches in both computational and statistical performance.

Keywords: Central limit theorem, Cross-validation, Graph dimension, Random graph

1 Introduction

In social network analysis, a large and popular class of models supposes that each person has a set of k latent characteristics and the probability that a pair of people are friends depends only on that pair’s k characteristics. Typically, for example, if two people have similar characteristics, then they are more likely to become friends. We aim to estimate the number of characteristics k using a class of models where every edge is statistically independent, conditionally on the characteristics. This includes the Latent Space Model, the Aldous-Hoover representation, and graphons [Hoff et al., 2002, Aldous, 1985, Hoover, 1989, Lovász, 2012, Jacobs and Clauset, 2014].

Denote the adjacency matrix $A \in \mathbb{N}^{n \times n}$ as recording the number of edges between i and j in element A_{ij} . We are particularly interested in the class of models where every person i is assigned a vector of characteristics $Z_i \in \mathbb{R}^k$ and

$$\mathbb{E}(A_{ij}) = \sum_{\ell=1}^k Z_{i\ell} Z_{j\ell} = \langle Z_i, Z_j \rangle. \quad (1)$$

This model is often called the random dot product model [Athreya et al., 2013], which includes the Stochastic Blockmodel, along with its degree-corrected and mixed membership variants [Karrer and Newman, 2011, Airoldi et al., 2008]. In the Stochastic Blockmodel, k is the number of blocks. Under mild identifiability conditions, $\mathbb{E}(A)$ and the normalized form of this matrix defined in Equation (2) below have k non-zero eigenvalues. We use this fact to estimate k .

The scree plot gives the sample eigenvalues. We look for an elbow or a gap.

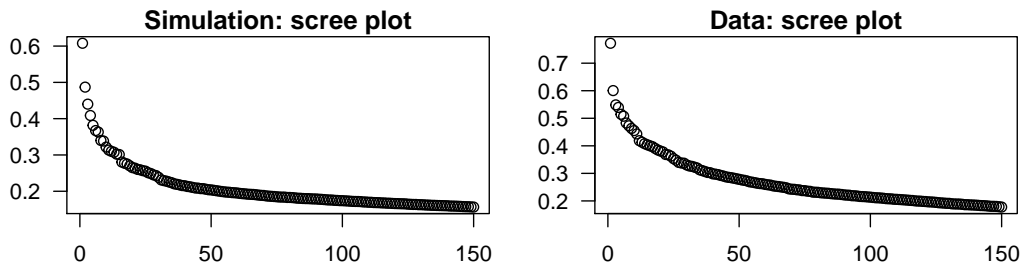


Figure 1: In these examples, it is difficult to detect a gap or elbow. In the left panel, the graph is simulated from a Degree-Corrected Stochastic Blockmodel with $n = 2560$. In the right panel, the graph is a citation graph among $n = 22,688$ academic journals. Displayed are the largest 150 eigenvalues of the normalized and regularized adjacency matrix, L , defined in Equation (2). Section 1.1 gives more details for these figures.

Unfortunately, the eigenvalues of A or of its normalized form (i.e., the “sample eigen-

values”) in the scree plot often fail to provide a clear estimate of k . As an illustration, this is the case in Figure 1. We address this problem with a cross-validation technique. There are three basic pieces that, when put together, enable our cross-validation approach to estimating the latent dimension k .

The *first piece* provides two identically distributed adjacency matrices, \tilde{A} and \tilde{A}_{test} , from a single adjacency matrix A . For each element i, j , define the elements of \tilde{A} and \tilde{A}_{test} as

$$\tilde{A}_{ij} \sim \text{Binomial}(A_{ij}, 1 - \varepsilon) \text{ and } [\tilde{A}_{\text{test}}]_{ij} = A_{ij} - \tilde{A}_{ij}.$$

If $\varepsilon = 1/2$, then \tilde{A} and \tilde{A}_{test} are identically distributed. If A has independent elements with $\mathbb{E}(A_{ij}) = \langle Z_i, Z_j \rangle$, then \tilde{A} also has independent elements with $\mathbb{E}(\tilde{A}_{ij}) = \langle Z_i, Z_j \rangle / (1 - \varepsilon)$. Moreover, we will model A_{ij} as Poisson, which makes \tilde{A} and \tilde{A}_{test} statistically independent. It is common to model A_{ij} as Poisson because it is convenient and, in sparse graphs specifically, the difference between the Poisson and Bernoulli models becomes negligible [Karrer and Newman, 2011, Flynn et al., 2020, Crane and Dempsey, 2018, Cai et al., 2016, Zhou and Amini, 2020]. See Section 5 for further comparison between Bernoulli and Poisson graphs.

The *second piece* is that $\mathbb{E}(A)$, $\mathbb{E}(\tilde{A})$, and $\mathbb{E}(\tilde{A}_{\text{test}})$ have nearly identical spectral properties that reveal k . Because $\mathbb{E}(\tilde{A}) = \mathbb{E}(A)/(1 - \varepsilon)$, dividing an eigenvalue of $\mathbb{E}(A)$ by $1 - \varepsilon$ gives an eigenvalue of $\mathbb{E}(\tilde{A})$. As a result, they have the same number of non-zero eigenvalues, which is the value k that we aim to estimate. Importantly, these matrices all have identical eigenvectors.

While the technical parts of the paper use the eigenvectors of an adjacency matrix, the proposed algorithm instead uses eigenvectors from the normalized and regularized adjacency matrices. To define this matrix for the full adjacency matrix A , define the node degrees $d_i = \sum_j A_{ij}$ and the regularization parameter $\tau = n^{-1} \sum_i d_i$. The normalized and regularized adjacency matrix is

$$L = DAD, \text{ where } D \text{ is a diagonal matrix with } D_{ii} = (d_i + \tau)^{-1/2}. \quad (2)$$

Importantly, the normalized and regularized form of $\mathbb{E}(A)$ also has k non-zero eigenvalues. For dense graphs, L has similar statistical properties to A . However, for sparse graphs, L has better statistical properties [Le et al., 2017, Zhang and Rohe, 2018].

The *third and final piece* of the proposed approach is that for an eigenvector \tilde{x} of \tilde{A} (or its normalized and regularized version \tilde{L}), the “cross-validated eigenvalue,”

$$\lambda_{\text{test}}(\tilde{x}) = \tilde{x}^T \tilde{A}_{\text{test}} \tilde{x} = \sum_{ij} \tilde{x}_i \tilde{x}_j [\tilde{A}_{\text{test}}]_{ij} \quad (3)$$

is a weighted sum of independent random variables which converges to the normal distribution; this result is conditional on \tilde{x} , which is independent of \tilde{A}_{test} in the Poisson model. We test whether the expected value of $\lambda_{\text{test}}(\tilde{x})$ is zero,

$$\mathbb{E}(\lambda_{\text{test}}(\tilde{x})|\tilde{A}) = \tilde{x}^T \mathbb{E}(\tilde{A}_{\text{test}}|\tilde{A})\tilde{x} = \tilde{x}^T \mathbb{E}(\tilde{A}_{\text{test}})\tilde{x} = \sum_{\ell} \left(\sum_i Z_{i\ell} \tilde{x}_i \right)^2 / 2. \quad (4)$$

When this value is zero, it means that \tilde{x} is orthogonal to the latent space; in this case, we say that \tilde{x} is not statistically useful (although, perhaps, it is still useful for tasks other than estimating Z_1, \dots, Z_n). Ideally, the first k eigenvectors will provide large values of λ_{test} , with large Z-scores, while the following eigenvectors have $\lambda_{\text{test}} \approx 0$ and Z-scores normally distributed, with mean zero and variance one. The main theoretical result, stated in Theorem 4.1 below, shows that the proposed technique is consistent.

1.1 Motivating examples

In Figure 1, the simulated graph comes from a Degree-Corrected Stochastic Blockmodel, with $k = 128$ hierarchically arranged blocks. Many of the 128 dimensions cannot be estimated from the data. As such, it is not surprising that no artifacts arise in the scree plot around 128.

In Figure 2 below, the simulated scree plot from Figure 1 is repeated as a black line. The first two eigenvalues have been removed to improve the display. The blue line gives $\tilde{x}^T \tilde{L}_{\text{test}} \tilde{x}$, where \tilde{x} runs through the leading 150 eigenvectors of \tilde{L} . The red line gives the population version of this quantity, where the normalized and regularized matrix is constructed from the matrix $\mathbb{E}(A)$. The red and blue lines reveal that the eigenvectors computed from the data do not correlate with the underlying Z 's after around $\hat{k} \approx 60$. Moreover, the Z-scores in the right panel start to cluster around the cutoff at $\hat{k} \approx 60$. The standard scree plot (black line in left panel) does not reveal anything around this value. The full details of this simulation model are provided in Appendix B.1. This illustration splits the edges ten separate times, each with probability $\varepsilon = .1$, and averages the results over those ten folds.

The right panel of Figure 1 gives the scree plot for a citation graph on 22,688 academic journals. This graph was constructed from the Semantic Scholar database [Ammar et al., 2018] of roughly 220 million academic papers. Citations from one paper to another were converted to citations between the journals that published the papers. If there were more than 5 citations from journal i to journal j using a 5% sample of all edges, then A_{ij} is set to one. Otherwise, A_{ij} is zero. This graph was originally constructed and studied in Rohe and Zeng [2020]. For simplicity, the graph was symmetrized by setting $A_{ij} = 1$ if $A_{ji} = 1$.

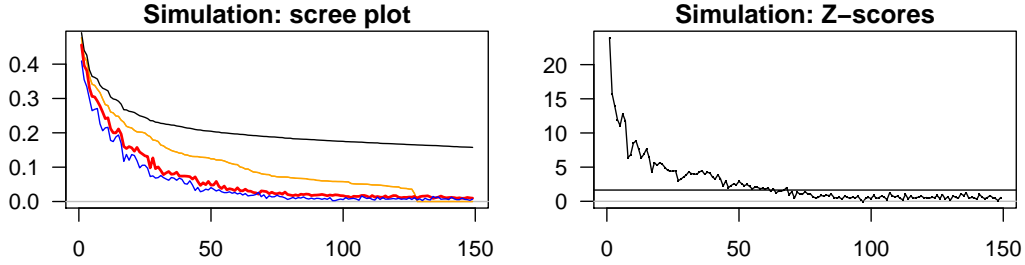


Figure 2: In the left panel, the black line gives the empirical eigenvalues (repeated from the left panel of Figure 1) and the orange line gives the $k = 128$ non-zero population eigenvalues. The blue line gives $\tilde{x}^T \tilde{L}_{\text{test}} \tilde{x}$ and red line gives the population version of this quantity. In the right panel, the Z-scores test the null hypothesis that the quantity in (4) is zero. The horizontal black line gives the cutoff for .05 significance. In this example, a good choice for \hat{k} would be around 60.

The average journal degree is 35. In the simulation in Figure 2 above, the red and orange lines give “population quantities,” constructed with $\mathbb{E}(A)$. In Figure 3, we use the blue line as an estimate of the red line and the Z-scores to test the null hypothesis that Equation (4) is equal to zero.

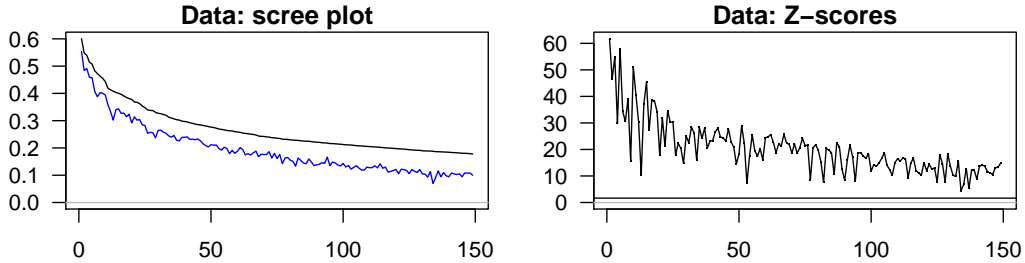


Figure 3: In this example, $\varepsilon = .05$ and for illustration, the data was divided only one time. All of the leading 150 dimensions are highly statistically significant. This is consistent with the results in Rohe and Zeng [2020] that showed the leading 100 dimensions reveal groups of journals that form coherent academic areas. In this example, L has 789,980 non-zero elements, spread across 22,688 rows and columns. Despite the relatively large size of this graph, computing all 150 cross-validated eigenvalues and their Z-scores requires less than 10 seconds in R on a 2020 MacBook Pro. This speed is enabled by the sparse matrix packages Matrix and RSpetra [Bates and Maechler, 2021, Qiu and Mei, 2019]

One way of understanding the difficulty of using spectral approaches for estimating k is this: the sample eigenvectors can “overfit” to the noise in large-scale graphs and it is hard to tell when this overfitting happens. This is the same overfitting that makes the sample eigenvalues in the scree plot differentially biased; in Figure 2 in the left panel, the gap

from the the black line to the orange and red lines is smaller on the left and larger on the right. In this paper, we exploit a notion of cross-validated eigenvalues as a new approach to estimating k . Here, the eigenvectors and cross-validated eigenvalues are computed on different graphs which is made possible by splitting the edges into two graphs [Abbe and Sandon, 2015, Abbe et al., 2016]. This removes the bias from overfitting.

Under a large class of random graph models, we provide a simple procedure to compute cross-validated eigenvalues.

A related holdout approach was previously explored in the econometrics literature [Abadir et al., 2014, Lam, 2016] for covariance estimation. In this paper and in those prior papers, the eigenvectors are estimated with a portion of the data and the “signal strength” of those vectors is estimated with the remaining held-out data. There are three key differences with this previous work. First, the observed data is of a different nature; for a covariance matrix $\Sigma \in \mathbb{R}^{p \times p}$, it is assumed in Lam [2016] that we observe $y_i = \Sigma^{1/2}x_i$, where x_i are unobserved and contain independent, identically distributed (i.i.d.) random variables. Second, the notion of sample splitting is different; the approach in Abadir et al. [2014] constructs a sample covariance matrix with a subsample of the observed vectors y_1, \dots, y_n . Third, the target of estimation is different; we provide p -values to estimate k , while the prior work aims to estimate the eigenvalues of Σ , which is presumed to be full rank.

For cross-validated eigenvalues, we provide an intuitive central limit theorem, which leads to a p -value for the statistical significance of a sample eigenvector. This can be used to estimate the number of statistically useful sample eigenvectors, and thus k . We provide consistency results for the proposed estimator of k , allowing for weighted and sparse graphs. Finally, through simulations and real data applications, we show that this estimator compares favorably to alternative approaches in both computational and statistical performance.

1.2 Prior literature

Numerous methods have been proposed to estimate k under the Stochastic Blockmodel and its degree-corrected version [Bordenave et al., 2015, Bickel and Sarkar, 2016, Lei, 2016, Wang and Bickel, 2017, Chen and Lei, 2018, Ma et al., 2019, Le and Levina, 2019, Liu et al., 2019, Jin et al., 2020]. One previous technique has been proposed to estimate the dimension of the more general random dot product graph [Li et al., 2020]. These methods roughly fall into one of three categories: spectral, cross-validation, and (penalized) likelihood-based approaches. Methods based on likelihood or cross-validation are actively researched, yet the majority of them are commonly restrained by the scale of networks. Spectral methods are

highly scalable for estimating k in large networks, although their rigorous analyses require delicate, highly technical random matrix arguments [Ajanki et al., 2017, Benaych-Georges et al., 2019, Chakrabarty et al., 2020, Dumitriu and Zhu, 2019, Benaych-Georges et al., 2020, Hwang et al., 2020].

Among the likelihood-based approaches, the authors of Wang and Bickel [2017] proposed to estimate k by solving a Bayesian information criterion (BIC) type optimization problem, where the objective function is a sum of the log-likelihood and of the model complexity. The computation is often not feasible because the likelihood contains exponentially many terms. In Ma et al. [2019], a pseudo-likelihood ratio is used to compare the goodness-of-fit of models with differing k s that have been estimated using spectral clustering with regularization [Rohe et al., 2011, Qin and Rohe, 2013, Joseph and Yu, 2016, Su et al., 2019], speeding up the computation. However, the two methods allow little node degree heterogeneity. Related to the goodness-of-fit technique, the authors of Jin et al. [2020] present a stepwise testing approach based on the number of quadrilaterals in the networks. Computing the statistic requires at least n^2 multiplication operations, regardless of the sparsity of the graph, thus is infeasible for large n . More recently, cross-validation [Picard and Cook, 1984, Arlot and Celisse, 2010] has also been adapted to the context of choosing k . For example, in Chen and Lei [2018], a block-wise node-pair splitting technique is introduced. In each fold, a block of rows of the adjacency matrix are held out from the Stochastic Blockmodel fitting (including the community memberships), then the left-out rows are used to calculate a predictive loss. In Li et al. [2020], the authors propose to hold out a random fraction of node-pairs, instead of nodes (thus all the incidental node-pairs). In addition, they suggest using a general low-rank matrix completion (e.g., a singular value thresholding approach [Chatterjee, 2015]) to calculate the loss on the left-out node-pairs. Theoretical conditions for not under-estimating k were established in both cross-validation based methods [Chen and Lei, 2018, Li et al., 2020]. Calculating the loss on either held-out rows or on scattered values in the adjacency matrix requires $O(n^2)$ computations, regardless of sparsity. This limits the ability of these techniques to scale to large graphs.

In Bickel and Sarkar [2016], Lei [2016], hypothesis tests using the top eigenvalue or singular value of a properly normalized adjacency matrix are proposed, based on edge universality and other related results for general Wigner ensembles [Tracy and Widom, 1994, Soshnikov, 1999, Erdős et al., 2012, 2013, Alex et al., 2014]. The analyses of these hypothesis tests assume dense graphs. In Liu et al. [2019], a version of the “elbow in the scree plot” approach (see, e.g., Zhu and Ghodsi [2006] for a discussion of this approach) is analyzed rigorously under the Degree-Corrected Stochastic Blockmodel, also in the dense case. For sparser graphs, the spectral properties of other matrices associated to graphs

have been used to estimate k , including the non-backtracking matrix [Krzakala et al., 2013, Bordenave et al., 2015, Le and Levina, 2019] and the Bethe-Hessian matrix [Le and Levina, 2019]. However, their theoretical analysis currently allow little node degree heterogeneity in the sparse case.

There is also related work on bootstrapping [Snijders and Borgatti, 1999, Thompson et al., 2016, Green and Shalizi, 2017, Levin and Levina, 2019, Lin et al., 2020a], jackknife resampling [Lin et al., 2020b] and subsampling [Bhattacharyya and Bickel, 2015, Lunde and Sarkar, 2019, Naulet et al., 2021] in network analysis. In particular, in Lunde and Sarkar [2019], subsampling schemes are applied to the nonzero eigenvalues of the adjacency matrix under low-rank graphon models. Weak convergence results are established under some technical conditions, including sufficient edge density (i.e., average degree growing asymptotically faster than \sqrt{n}); simulation results also indicate that sparsity leads to poor performance for the estimators considered, especially in the case of the eigenvalues closer to the bulk.

2 The statistical model, sample eigenvalues, and a new measure of signal strength

We consider a connected multigraph $G = (V, E)$ consisting of the set of nodes $V = \{1, \dots, n\}$ and edges E , where we allow multiple edges and self-loops. The adjacency matrix $A \in \mathbb{N}^{n \times n}$ records the number of edges between i and j in element A_{ij} .

The introduction motivated the paper by expressing $\mathbb{E}(A_{ij}) = \langle Z_i, Z_j \rangle$ in Equation (1). If the $Z_1, \dots, Z_n \in \mathbb{R}^k$ span \mathbb{R}^k and the elements A_{ij} are independent Poisson variables, then this model is included in Definition 1, which is the focus of this paper.

Definition 1 (Poisson graph). *We consider random graph models where the elements of A are independent Poisson random variables and $\mathbb{E}(A)$ has the eigendecomposition*

$$\mathbb{E}(A) = U\Lambda U^T \tag{5}$$

for $U \in \mathbb{R}^{n \times k}$ with orthonormal columns and diagonal matrix $\Lambda \in \mathbb{R}^{k \times k}$ with positive elements $\lambda_1, \dots, \lambda_k \in \mathbb{R}$ down the diagonal in non-increasing order.

Define the population (or expectation) matrix $P = \mathbb{E}(A)$. The diagonal of Λ contains the leading k eigenvalues of P and their corresponding eigenvectors are in the columns of U . For $j > k$, the eigenvalues of P are $\lambda_j = 0$. In this paper, we aim to estimate the number of nonzero eigenvalues.

This paper makes two simplifying assumptions. The first simplifying assumption is that A is symmetric (i.e., edges are undirected). This assumption can be relaxed; Remark 4.3 discusses directed graphs, contingency tables, and rectangular incidence matrices. The second simplifying assumption is that the elements of A are Poisson. A simulation in Section 5 demonstrates that the proposed technique provides reliable p -values in Bernoulli graphs as well.

2.1 Sample eigenvalues: a poor diagnostic

A common approach to estimating the eigenvalues of P is to use a plug-in estimator, i.e., estimating the eigenvalues of P with the eigenvalues of A . The symmetric matrix $A \in \mathbb{N}^{n \times n}$ has eigenvectors $\hat{x}_1, \dots, \hat{x}_n \in \mathbb{R}^n$ that are the solution to

$$\hat{x}_j = \operatorname{argmax}_{x \in \hat{S}_j} x^T A x, \quad (6)$$

where $\hat{S}_j = \{x \in \mathbb{R}^n : \|x\|_2 = 1 \text{ and } x^T \hat{x}_\ell = 0 \text{ for } \ell = 1, \dots, j-1\}$. The eigenvalues $\hat{\lambda}_j$ for $j = 1, \dots, n$ are defined as

$$\hat{\lambda}_j = \hat{x}_j^T A \hat{x}_j. \quad (7)$$

Note that the quadratic form that defines the eigenvalues in Equation (7) is identical to the objective function that the eigenvectors optimize in equation (6). This leads to overfitting and bias.

The eigenvalues of A , i.e., $\hat{\lambda}_1, \hat{\lambda}_2, \hat{\lambda}_3, \dots$, are often plotted against their index $1, 2, 3, \dots$. This is called a scree plot and it is used as a diagnostic to estimate k . In this scree plot, there might be a “gap” or an “elbow” at the k th eigenvalue, which reveals k .

However, there is a fundamental problem with the plug-in estimator for the population eigenvalues which can make the “gap” or “elbow” in the scree plot more difficult to observe. The leading eigenvalue estimates $\hat{\lambda}_1, \dots, \hat{\lambda}_k$ are asymptotically unbiased, so long as their corresponding population eigenvalues $\lambda_1, \dots, \lambda_k$ are large enough (see, e.g., Chakrabarty et al. [2020] for related results). However, when n is much larger than k , $\hat{\lambda}_{k+1}$ is a biased estimate of $\lambda_{k+1} = 0$, with $\mathbb{E}(\hat{\lambda}_{k+1}) > \lambda_{k+1} = 0$ (see, e.g., Benaych-Georges et al. [2020] for related results). So, if λ_k is not large enough, then this bias diminishes the appearance of a “gap” or “elbow” between $\hat{\lambda}_k$ and $\hat{\lambda}_{k+1}$ in the scree plot.

This can be seen in the left panel of Figure 2. In that figure, the gap between the sample eigenvalues (black line) and the population eigenvalues (orange line) is smaller on the left and larger on the right. Note that in this figure, it is not the eigenvalues of A and $\mathbb{E}(A)$ that are shown, but rather the eigenvalues of the normalized and regularized forms

of A and $\mathbb{E}(A)$.

2.2 Measuring the signal strength of a sample eigenvector

Even if an oracle were to tell us that the population eigenvector x_j has population eigenvalue $\lambda_j \neq 0$, we should only use the sample eigenvector \hat{x}_j for statistical inference if \hat{x}_j is close to x_j and other leading population eigenvectors. Because of this requirement, the population eigenvalues λ_j do not measure the signal strength of \hat{x}_j .

In the realistic setting where the signal is not overwhelming for every sample eigenvector \hat{x}_j for $j < k$, we will measure the signal strength of this vector in the following way. Define the population (or expected) cross-validated eigenvalue of a sample eigenvector \hat{x}_j as

$$\lambda_P(\hat{x}_j) = \hat{x}_j^T P \hat{x}_j. \quad (8)$$

Of course, this is not actually an eigenvalue in the traditional sense. However, there are three reasons to think of this quantity as an analogue. First, the quadratic form in Equation (8) mimics the form for the sample eigenvalue in Equation (7), which is also the objective function that the sample eigenvectors optimize in Equation (6). As such, for a population eigenvector x_j , $\lambda_P(x_j)$ is the corresponding population eigenvalue λ_j .

The second reason to think of λ_P as an analogue of an eigenvalue is that for a sample eigenvector \hat{x} , there always exists a vector $\hat{x}^\perp \in \mathbb{R}^n$ that is orthogonal to \hat{x} and

$$P\hat{x} = \hat{\lambda}\hat{x} + \hat{x}^\perp$$

for some value $\hat{\lambda} \in \mathbb{R}$. If $\hat{x}^\perp = 0$, then \hat{x} is an eigenvector of P with eigenvalue $\hat{\lambda}$. Even when $\hat{x}^\perp \neq 0$, if $\|\hat{x}\|_2 = 1$, then $\hat{\lambda} = \lambda_P(\hat{x})$.

$$\lambda_P(\hat{x}) = \hat{x}^T P \hat{x} = \hat{x}^T (\hat{\lambda}\hat{x} + \hat{x}^\perp) = \hat{\lambda}$$

The third reason also provides intuition for why λ_P is a measure of signal strength; indeed λ_P provides for the optimal reconstruction of P as conceptualized in the following proposition. See Section A for a proof.

Proposition 2.1 (Lam [2016]). *The solution to*

$$\min_{\hat{\lambda}_1, \dots, \hat{\lambda}_q} \left\| P - \sum_{j=1}^q \hat{\lambda}_j \hat{x}_j \hat{x}_j^T \right\|_F$$

is $\hat{\lambda}_j = \lambda_P(\hat{x}_j)$ for $j = 1, \dots, q$.

A key advantage of the population quantity $\lambda_P(\hat{x}_j)$ over λ_j is that it reveals information about the vector that we can compute, i.e., \hat{x}_j , not the eigenvector that we wish we had, i.e., x_j . If a sample eigenvector \hat{x}_j is close to its population counterpart x_j , then for the reasons above, it is reasonable to presume that $\lambda_P(\hat{x}_j)$ is close to the population eigenvalue λ_j . However, if the estimation problem is too difficult and \hat{x}_j is nearly orthogonal to the eigenvectors of P that have non-zero eigenvalues, then $\lambda_P(\hat{x}_j) \approx 0$. Notably, and most importantly, this can happen even if \hat{x}_j 's corresponding population eigenvector x_j has a non-zero eigenvalue. For example, this happens when the estimation problem is too difficult as happens for the 60th-128th sample eigenvectors in Figure 2.

The notion of $\lambda_P(\hat{x}_j)$ was originally proposed and studied in [Abadir et al. \[2014\]](#) and [Lam \[2016\]](#) for optimal estimation of eigenvalue shrinkage under a different statistical model. While the signal strength λ_P is unknown, cross validation can provide an unbiased estimator that is asymptotically normal. The next three sections develop and study a statistical testing procedure for the null hypothesis

$$H_0 : \lambda_P(\tilde{x}_j) = 0 \tag{9}$$

conditionally on \tilde{x}_j , where \tilde{x}_j are estimates of the eigenvectors of P (or its normalized form) constructed from a large subsample of the edges in the graph.

3 The three key pieces for cross-validated eigenvalues

This section details the three key pieces that enable the estimation of cross-validated eigenvalues. First, edge splitting a Poisson random graph creates two independent Poisson random graphs. Second, the expected adjacency matrices of the resulting graphs are “spectrally invariant” to this edge splitting. Third, the quadratic form for λ_{test} in Equation (3) satisfies a central limit theorem.

3.1 The first piece: edge splitting creates independent Poisson graphs

The ES procedure in Algorithm 1 splits the edges of a graph into two graphs and outputs the two adjacency matrices \tilde{A} and \tilde{A}_{test} . Notice that under ES and conditionally on A_{ij} , $\tilde{A}_{ij} \sim \text{Binomial}(A_{ij}, \varepsilon)$ and $[\tilde{A}_{\text{test}}]_{ij} = A_{ij} - \tilde{A}_{ij}$. The independence of \tilde{A} and \tilde{A}_{test} follows from the next lemma, often referred to as thinning (see, e.g., [Durrett \[2019, Section 3.7.2\]](#)).

Lemma 3.1. Define $X \sim \text{Poisson}(\lambda)$ and conditionally on X , define $Y \sim \text{Binomial}(X, p)$ and $Z = X - Y$. Unconditionally on X , the random variables Y and Z are independent Poisson random variables and, further, $Y \sim \text{Poisson}(p\lambda)$ and $Z \sim \text{Poisson}((1 - p)\lambda)$.

To apply the lemma, let X be A_{ij} , let λ be P_{ij} , let Y and Z be the (i, j) -th elements of \tilde{A} and \tilde{A}_{test} respectively, and let $p = \varepsilon$. Lemma 3.1 implies that \tilde{A} and \tilde{A}_{test} are independent Poisson random graphs.

Input: Adjacency matrix $A \in \mathbb{N}^{n \times n}$ and edge splitting probability $\varepsilon \in (0, 1)$.

Procedure $\text{ES}(A, \varepsilon)$:

1. Convert A into $G = (V, E)$, where $\{i, j\}$ is repeated in the edge set E potentially more than once if $A_{ij} > 1$.
2. Initiate \tilde{E}_{test} and \tilde{E} , two empty edge sets on V .
3. **for** each copy of edge $\{i, j\} \in E$ **do**
 assign it to \tilde{E}_{test} with probability ε . Otherwise, assign it to \tilde{E} .
4. Convert $(V, \tilde{E}_{\text{test}})$ into an adjacency matrix $\tilde{A}_{\text{test}} \in \mathbb{N}^{n \times n}$ and (V, \tilde{E}) into an adjacency matrix $\tilde{A} \in \mathbb{N}^{n \times n}$.

Output: \tilde{A} and \tilde{A}_{test} .

Algorithm 1: Edge splitting

3.2 The second piece: the population graphs are “spectrally invariant” to splitting

The next proposition shows that ES preserves the spectral properties of the population adjacency matrices $\mathbb{E}(\tilde{A})$ and $\mathbb{E}(\tilde{A}_{\text{test}})$. This result does not require any distributional assumptions on A , only that its elements are integers (so that \tilde{A} and \tilde{A}_{test} are defined).

Proposition 3.1. *If \tilde{A} and $\tilde{A}_{\text{test}} \in \mathbb{N}^{n \times n}$ are generated by applying ES to $A \in \mathbb{N}^{n \times n}$ with splitting probability ε , then*

1. *The eigenvectors of $\mathbb{E}(A)$, $\mathbb{E}(\tilde{A})$, and $\mathbb{E}(\tilde{A}_{\text{test}})$ are identical.*
2. *If λ_j is an eigenvalue of $\mathbb{E}(A)$, then $(1 - \varepsilon)\lambda_j$ is an eigenvalue of $\mathbb{E}(\tilde{A})$ and $\varepsilon\lambda_j$ is an eigenvalue of $\mathbb{E}(\tilde{A}_{\text{test}})$.*

Here, all expectations are unconditional on A .

Proof. Define $P = \mathbb{E}(A)$ and let $P = U\Lambda U^T$ be its eigendecomposition; if A is not random, then $P = A$ and U, Λ potentially have n columns. It follows directly from the construction

in ES that $\mathbb{E}(\tilde{A}) = (1 - \varepsilon)P$ and $\mathbb{E}(\tilde{A}_{\text{test}}) = \varepsilon P$. Rearranging terms reveals the eigendecomposition of $\mathbb{E}(\tilde{A}_{\text{test}})$,

$$\mathbb{E}(\tilde{A}_{\text{test}}) = \varepsilon P = U(\varepsilon\Lambda)U^T$$

and similarly for $\mathbb{E}(\tilde{A})$. This shows that they have the same eigenvectors and the simple relationship between their eigenvalues in the statement. \square

3.3 The third piece: cross-validated eigenvalues are asymptotically Gaussian

To state the theorem formally, we consider a sequence of random adjacency matrices $B^{(n)} \in \mathbb{N}^{n \times n}$ from Poisson random graphs with $\mathbb{E}(B^{(n)}) = Q^{(n)} \in \mathbb{R}^{n \times n}$ satisfying $\max_{ij} Q_{ij}^{(n)} \leq 1$, and a sequence of unit vectors $x^{(n)} \in \mathbb{R}^n$. To simplify the notation, we suppress the explicit dependence on n . We will impose the following delocalization condition on x :

$$\|x\|_{\infty}^2 = o(\sigma), \tag{10}$$

where

$$\sigma^2 = 2(x^2)^T Q(x^2) - (x^2)^T \text{diag}(Q)(x^2),$$

with x^2 being the vector x with entries squared and $\text{diag}(Q)$ being the diagonal matrix containing the diagonal elements of Q . Similarly, we also define

$$\hat{\sigma}^2 = 2(x^2)^T B(x^2) - (x^2)^T \text{diag}(B)(x^2).$$

In the next section, we will apply the theorem to $B := \tilde{A}_{\text{test}}$, $Q := \varepsilon P$ and x an eigenvector of \tilde{A} or of its normalized form.

Theorem 3.1 (CLT for cross-validated eigenvalue). *Let B , Q , σ and $\hat{\sigma}$ be as above. Assume that x satisfies Condition (10). Then,*

$$\frac{\lambda_B(x) - \lambda_Q(x)}{\hat{\sigma}} \Rightarrow N(0, 1). \tag{11}$$

The proof of Theorem 3.1 is in Appendix A.

Remark 3.1. *If the elements of B are Bernoulli instead of Poisson, then a similar central limit theorem holds with a new variance γ^2 that contains the sum $\sum_{ij} x_i^2 x_j^2 P_{ij}(1 - P_{ij})$. The key difference compared to the Poisson variance is the inclusion of $(1 - P_{ij})$ which is difficult to estimate. Because $(1 - P_{ij}) \leq 1$, The Poisson model formula for σ^2 provides an*

upper bound for γ^2 . As such, σ^2 and $\hat{\sigma}^2$ can still be used to provide conservative inference. Moreover, when the graph is sparse, we have $(1 - P_{ij}) \rightarrow 1$ and σ^2 , and $\hat{\sigma}^2$ become better approximations. The key problem with Bernoulli graphs is not the lack of normality, or estimating the variance. The key problem is that \tilde{A} and \tilde{A}_{test} are no longer independent. So the CLT in Theorem 3.1 cannot be applied to $\hat{\lambda}(\tilde{x})$ if A contains Bernoulli elements. This is further discussed and studied in Section 5.

Remark 3.2. Regarding the delocalization condition (10), when all entries of Q are of the same order $\rho = o(1)$, then $\sigma = \Theta(\rho^{1/2})$ and the condition boils down to $\|x\|_\infty = o(\rho^{1/4})$. In Appendix A.2.1 (Corollary A.1), we discuss a sufficient condition for $\|x\|_\infty^2 = o(\sigma)$ to hold in terms of the expected number of edges in B .

4 Cross-validated eigenvalue estimation

In this section, we use Theorem 3.1 to test the null hypothesis $H_0 : \lambda(\tilde{x}_j) = 0$, where \tilde{x}_j is an eigenvector of \tilde{A} . Section 4.1 states the algorithm and Section 4.2 provides the main theoretical result, i.e., that it is consistent.

4.1 The algorithm

The algorithm reports a p -value for each eigenvector. These are then used to estimate k . In addition to the splitting probability ε , the algorithm takes two more parameters: (i) the maximum number k_{max} of eigenvectors to consider and (ii) the significance level α . We describe the algorithm for an undirected graph with the adjacency matrix $A \in \mathbb{N}^{n \times n}$ in Algorithm 2; see Remark 4.3 for rectangular or asymmetric A . After EigCV, a few remarks on the theory and the implementation are in order.

Remark 4.1. Theorem 4.1 studies EigCV with $\text{folds} = 1$ and \tilde{A} instead of \tilde{L} in step ii. Moreover, there is an additional step needed in Theorem 4.1 to check for delocalization. This technical requirement is further discussed in Section 4.2. This step is not used in EigCV or in our code. We allow for these modifications in EigCV because they are practically advantageous. Increasing $\text{folds} > 1$ helps to remove the randomness in the p -values generated from edge splitting ES (see Section B.2.2 for further discussion of $\text{folds} > 1$). Using \tilde{L} instead of \tilde{A} helps reduce localization of eigenvectors [Le et al., 2017, Zhang and Rohe, 2018]. Finally, we do not include a check for delocalization because we find in the simulation in Section 5 that when an eigenvector \tilde{x}_ℓ delocalizes, then $(\tilde{x}_\ell^2)^\top A \tilde{x}_\ell^2$ in the formula for $\tilde{\sigma}_\ell$ is very large, thus leading to conservative inferences.

Input: Adjacency matrix $A \in \mathbb{N}^{n \times n}$, edge splitting probability $\varepsilon \in (0, 1)$, and significance level $\alpha \in (0, 1)$

Procedure EigCV(A, ε, k_{\max} , folds):

1. **for** $f = 1, \dots$, folds **do**
 - i. $\tilde{A}, \tilde{A}_{\text{test}} \leftarrow \text{ES}(A, \varepsilon)$ // Algorithm 1
 - ii. (Optional) Compute \tilde{L} with \tilde{A} as in Equation (2).
 - iii. Compute the leading k_{\max} eigenvectors of \tilde{L} (or \tilde{A}), as $\tilde{x}_1, \dots, \tilde{x}_{k_{\max}}$.
 - iv. **for** $\ell = 2, \dots, k_{\max}$ **do**
compute the test statistic

$$T_{f,\ell} = \frac{\tilde{\lambda}_{\text{test}}(\tilde{x}_\ell)}{\tilde{\sigma}_\ell},$$

where $\tilde{\lambda}_{\text{test}}(x) = x^T \tilde{A}_{\text{test}} x$, and $\tilde{\sigma}_\ell = \sqrt{2\varepsilon(\tilde{x}_\ell^2)^T A \tilde{x}_\ell^2 - \varepsilon(\tilde{x}_\ell^2)^T \text{diag}(A) \tilde{x}_\ell^2}$ is the standard error evaluated using the full graph. Here, $\tilde{x}_\ell^2 \in \mathbb{R}^n$ is the vector \tilde{x}_ℓ with each element squared.

2. **for** $\ell = 2, \dots, k_{\max}$ **do**
Compute T_ℓ as the mean of the $T_{1,\ell}, \dots, T_{\text{folds},\ell}$ and compute the one-sided p -value $p_\ell = 1 - \Phi(T_\ell)$, where Φ is the cumulative distribution function of the standard normal distribution.

Output: The graph dimensionality estimate: $\text{argmin}_{k \leq k_{\max}} \{p_k \geq \alpha\} - 1$.

Algorithm 2: Eigenvalue cross-validation

Remark 4.2. *If folds = 1 and the p-values p_k are used to select eigenvectors, then the eigenvectors \tilde{x}_k should be used (not \hat{x}_k). This is because the p-value p_k is only associated with the eigenvector \tilde{x}_k . It is tempting to compute the eigenvectors of A or L with all of the edges and then give the k -th eigenvector \hat{x}_k the p-values p_k . However, when the left-out edges are also used to compute the eigenvectors, this alters the eigenvectors. In addition to slightly changing the elements of the eigenvectors, it is common for the order of the eigenvectors to also change. Or, for the new eigenvectors to be a more general rotation of the subsampled eigenvectors. It is an area for future research to understand if and how the p-values can be extended. By making ε small we can ensure that the subsampled eigenvectors \tilde{x}_k are nearly as good as \hat{x}_k .*

EigCV easily extends to two other settings, rectangular incidence matrices and a test of independence for contingency tables.

Remark 4.3. Rectangular incidence matrices. *If the matrix $A \in \mathbb{N}^{r \times c}$ is either rectangular or asymmetric (e.g., the adjacency matrix for a directed graph, the incidence matrix for a bipartite graph, a contingency table, etc.), then eigenvectors should be replaced by singular vectors. In step 3 of EigCV, compute the singular vector pairs \tilde{u}_ℓ and \tilde{v}_ℓ . Then, the test statistic is*

$$T_\ell = \frac{\tilde{u}_\ell^\top \tilde{A}_{\text{test}} \tilde{v}_\ell}{\sqrt{\varepsilon (\tilde{u}_\ell^2)^\top A \tilde{v}_\ell}}.$$

Theorem 3.1 extends under analogous conditions to this setting. Our R package (<https://github.com/RoheLab/gdim>) includes this extension.

Remark 4.4. Contingency tables. *Suppose $A \in \mathbb{N}^{r \times c}$ is a contingency table with multinomial elements. Note that the χ^2 test of independence tests the null hypothesis that $\mathbb{E}(A)$ is rank 1, i.e., $k = 1$. To test if $\mathbb{E}(A)$ has rank greater than $k = 1$ and potentially reject independence, one can apply EigCV to A with $k_{\text{max}} = 2$, using the extension to rectangular matrices in Remark 4.3. The three key pieces for the cross-validation apply to this setting, thus enabling this approach. First, if the distribution of A is multinomial, then ES provides two independent matrices. Second, in expectation, those matrices have identical singular vectors and the same number of non-zero singular values. Third, the CLT in Theorem 3.1 extends to this data generating model with analogous conditions. EigCV is potentially powerful for alternative hypotheses where $\mathbb{E}(A)$ has a large second eigenvalue. In contrast to the traditional Pearson's χ^2 test for independence, EigCV handles a large number of rows and columns and a sparse A , where the vast majority of elements are zeros. Moreover, it has the added advantage that the singular vectors \tilde{u}_2 and \tilde{v}_2 estimate where the deviation from independence occurs, thus making the results more interpretable. This is an area of our ongoing research.*

4.2 Statistical consistency

This section states a consistency result for a modified version of the algorithm stated in Algorithm 3 in Appendix A.3. The main modification is the addition of a delocalization test. We use K for the true latent dimension and \hat{K} for its estimate.

We will make some further assumptions. Let $P = \rho_n P^0$, where $0 < \rho_n < 1$ controls the sparsity of the network, and $P^0 = U \Lambda^0 U^T$ is a matrix of rank k with $P_{ij}^0 \leq 1$ for all i, j . Here, $\Lambda^0 = \text{diag}(\lambda_1^0, \dots, \lambda_K^0)$ is the diagonal matrix of its non-increasing eigenvalues, and $U = (u_1, \dots, u_K)$ contains the corresponding eigenvectors. We first consider the signal strength in the population adjacency matrix. The magnitude of the leading eigenvalues characterize the useful signal in the data; only if they are sufficiently large is it possible to identify them from a finite graph sample. As such, the first assumption requires that the leading eigenvalues of the population graph are of sufficient and comparable magnitude. We also include necessary assumptions on the sparsity of the graph.

Assumption 1 (Signal strength and sparsity). *We assume that there exist positive constants ψ_1, ψ'_1 such that*

$$\kappa := \lambda_1^0 / \lambda_K^0 \in (0, \psi_1), \quad \lambda_1^0 \geq \psi'_1 n.$$

In addition, we assume that $P_{ij}^0 \leq 1$ for all i, j and that the network sparsity satisfies $c_0 \frac{\log^{\xi_0} n}{n} \leq \rho_n \leq c'_0 n^{-\xi_1}$, for some constants $\xi_0 > 2$, $\xi_1 \in (0, 1)$, $c_0, c'_0 > 0$.

Observe that Assumption 1 implies in particular that $\psi_1^{-1} \psi'_1 n \rho_n \leq \lambda_K \leq \lambda_1 \leq n \rho_n$ since $\lambda_1 \leq \text{tr}(P) \leq n \rho_n$. Assumption 1 is less strict than the assumptions in Li et al. [2020]. This is because we do not require a minimum gap between distinct eigenvalues, which is hard to satisfy in practice.

Next, we consider a property of the population eigenvectors. The notion of coherence was previously introduced by Candès and Recht [2009]. Under the parametrization of Assumption 1, the coherence of U is defined as

$$\mu(U) = \max_{i \in [n]} \frac{n}{K} \|U^T e_i\|^2 = \frac{n}{K} \|U\|_{2, \infty}^2,$$

where e_i is the i -th standard basis vector. A lower coherence indicates that the population eigenvectors are more spread-out—that is, they are not concentrated on a few coordinates.

Assumption 2 (Coherence). *We assume $\mu(U) \leq \mu_0$, for some constant $\mu_0 > 1$.*

Our main theoretical result asserts the consistency of our cross-validated eigenvalue

estimator for estimating the latent dimension. The proof of Theorem 4.1 is in Appendix A.

Theorem 4.1 (Consistency). *Suppose $A \in \mathbb{R}^{n \times n}$ is a Poisson graph satisfying Assumptions 1 and 2. Let K be the true latent space dimension, and let \hat{K} be the output of Algorithm 3 (see Appendix A.3) with edge splitting probability ε . Then,*

$$\mathbb{P}(\hat{K} = K) \rightarrow 1 \quad \text{as } n \rightarrow \infty.$$

5 Poisson vs Bernoulli

The Poisson model has previously been used to study statistical inference with random graphs [Karrer and Newman, 2011, Flynn et al., 2020, Crane and Dempsey, 2018, Cai et al., 2016, Zhou and Amini, 2020]. In the sparse graph setting, these models produce very similar graphs (e.g. Theorem 7 in Rohe et al. [2018]). Moreover, under the Poisson model, the edges are exchangeable [Cai et al., 2016, Crane and Dempsey, 2018, Rohe et al., 2018].

This section shows that EigCV continues to perform well in settings where the elements of A are Bernoulli random variables. The technical results and derivations in this paper do not directly apply to this setting. The key difficulty comes from the edge splitting. Under the Bernoulli model, $A_{ij} \in \{0, 1\}$. So, it is not possible for both \tilde{A} and \tilde{A}_{test} to get the edge i, j . This creates *negative* dependence. Because the fitting and test graph are dependent, a central limit theorem akin to Theorem 3.1 becomes more difficult. Nevertheless, a theorem akin to Theorem 4.1 still holds with minor changes to the conditions.

This simulation shows that the negative dependence created from Bernoulli edges makes the testing procedure more conservative. That is, when we are testing

$$H_0 : \mathbb{E}(\lambda_{\text{test}}(\tilde{x}_\ell)) = 0$$

for $\ell > k$, the $\alpha = .05$ test rejects with probability less than .05. This type of miscalibration is traditionally considered acceptable.

This section simulates from a $k = 2$ Stochastic Blockmodel and examines the distribution of T_3 and T_4 , under both the Bernoulli and Poisson models for edges. In all of these simulations, there are $n = 2000$ nodes. Each node is randomly assigned to either block 1 or 2 with equal probabilities. Let i and j be any two nodes in the same block and u and v be any two nodes in different blocks. Across simulation settings, $P_{ij}/P_{u,v} = 2.5$. While keeping this ratio constant, the values in P increase to make the expected degree of the

graph go from 3.5 to 105, by increments of 3.5. In the Poisson model, $A_{ij} \sim \text{Poisson}(P_{ij})$ and in the Bernoulli model, $A_{ij} \sim \text{Bernoulli}(P_{ij})$. We compute T_3 and T_4 in EigCV (Algorithm 2) with edge split probability $\varepsilon = .05$ and folds = 1. Appendix B.2.2 gives the identical simulation, but for folds = 10.

We use the one-sided rejection region $T_\ell > 1.65$. If $T_\ell \sim N(0, 1)$, then this has level $\alpha = .05$. We refer to the simulated probability that $T_\ell > 1.65$ as the rejection probability. Figure 4 estimates the rejection probability in two ways. First, each dot gives the proportion of 1000 replicates in which $T_\ell > 1.65$. Second, the line gives the values

$$\hat{\alpha} = 1 - \Phi((1.65 - \bar{T}_\ell)/\text{SD}(T_\ell)), \tag{12}$$

where Φ is the cumulative distribution function (CDF) of the standard normal, \bar{T}_ℓ is the average value of T_ℓ over the 1000 replicates, and $\text{SD}(T_\ell)$ is the standard deviation of these 1000 replicates. This is an estimate of the rejection probability, under the assumption that T_ℓ is normally distributed.

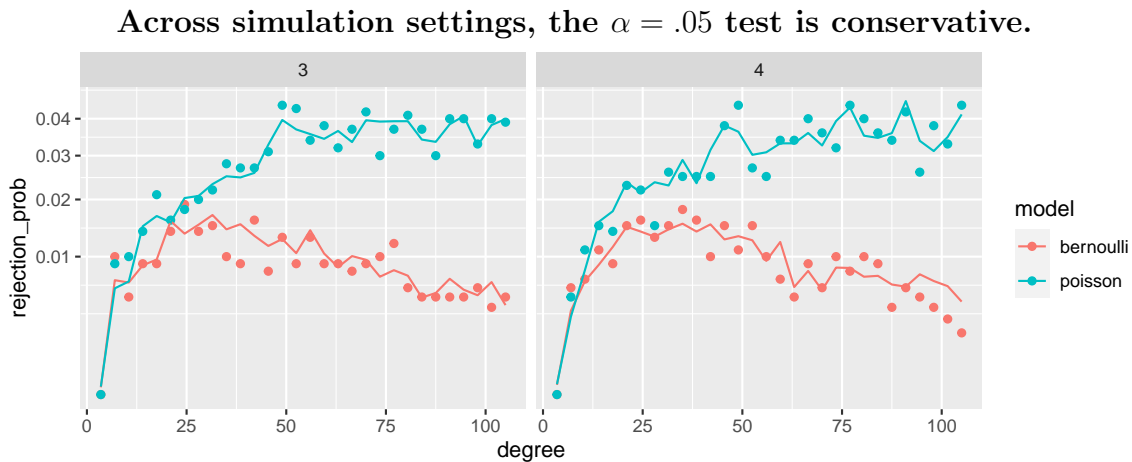


Figure 4: The left panel gives results for T_3 and the right panel gives results for T_4 . Each point corresponds to the proportion of 1000 replicates that the test statistic was greater than 1.65. The line is a smoothed version of $\hat{\alpha}$.

Under the simulation settings described above, Figure 4 shows four things.

1. The points and lines are below .05. So, the proposed test is conservative.
2. On the left side of both panels, the points and lines are well below .05. So, the proposed test is particularly conservative for very sparse graphs. Note that the bottom left point in both figures is over-plotted with two points. This is because none of the

4000 tests in the lowest degree graphs were rejected. The corresponding $\hat{\alpha}$'s are on the order 1/20,000.

3. On the right side of both panels, the red line decreases. So, for Bernoulli graphs, the test is increasingly conservative for denser graphs.
4. The points are scattered around their respective lines, which suggests that the normal distribution provides a reasonable approximation for the right tail of the distribution (but T_ℓ does not have expectation zero and variance one).

The test is increasingly conservative for dense Bernoulli graphs. In particular, the line giving the normal approximation $\hat{\alpha}$ is decreasing. So, either $\mathbb{E}(T_3) < 0$ or $\text{Var}(T_3) < 1$ or both (and similarly for T_4). The next figure, Figure 5, shows that the expectation of T_3 and T_4 decreases away from zero for dense Bernoulli graphs.

Under the Bernoulli model, for $\ell > k$, the negative dependence makes the expectation of T_ℓ decrease away from zero as the graph becomes more dense.

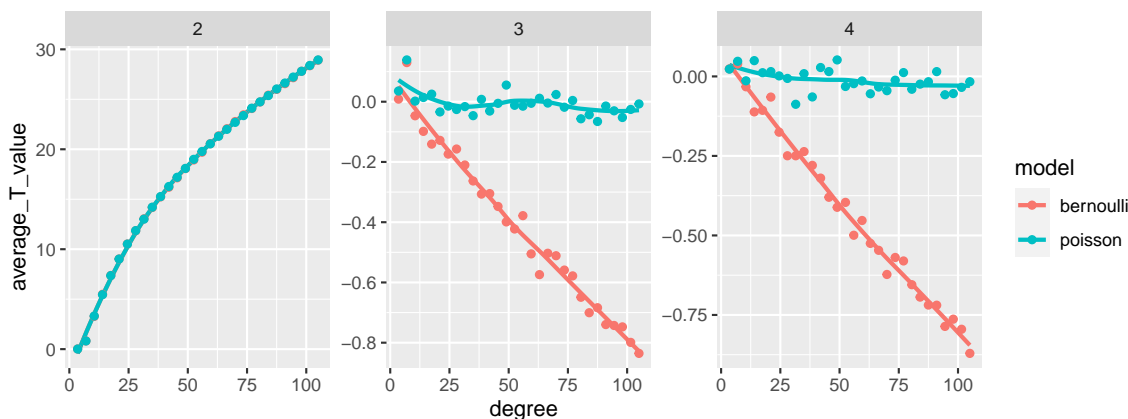


Figure 5: Each dot gives the average value of T_ℓ over 1000 replicates; T_2 on the left, T_3 in the middle, and T_4 on the right. The previous figure, Figure 4, shows that as the Bernoulli graph becomes denser, T_3 and T_4 are less likely to exceed 1.65. This figure shows that this is because their expectation decreases away from zero.

The expected values of T_3 and T_4 decrease due to the negative dependence between \tilde{A} and \tilde{A}_{test} under the Bernoulli model. That is, if an edge appears in \tilde{A} , then it cannot appear in \tilde{A}_{test} , and vice versa. Figure 5 shows that $\tilde{x}_\ell^T \tilde{A} \tilde{x}_\ell$ and $\tilde{x}_\ell^T \tilde{A}_{\text{test}} \tilde{x}_\ell$ are negatively correlated when (1) the edges are Bernoulli, (2) the graph is dense, (3) and $\ell > k$. In the two-block Stochastic Blockmodel, this negative dependence does not shift the expectation of T_2 , even for dense Bernoulli graphs (see also Figure 8 in Appendix B). The fact that \tilde{x}_ℓ displays negative correlation, but only for $\ell > k$, is particularly interesting. Here is one

interpretation: because these eigenvectors do not estimate signal, they only find noise in \tilde{A} . Then, that noise disappears in \tilde{A}_{test} due to the negative dependence.

On the very left of both panels in Figure 4, the expected degree is 3.5. In this very sparse regime, which is below the weak recovery threshold [Mossel et al., 2015] (see also Abbe [2018]), the test are conservative for both Bernoulli and Poisson graphs. In this very sparse regime, the eigenvectors \tilde{x}_ℓ often localize on a few nodes that have a large degree simply due to chance. When this happens, $(\tilde{x}_\ell^2)^T A \tilde{x}_\ell^2$ over-estimates the population quantity $(\tilde{x}_\ell^2)^T \mathbb{E}(A) \tilde{x}_\ell^2$. This causes $\tilde{\sigma}_\ell$ in the denominator of T_ℓ to be large, thus making the standard deviation of T_ℓ small and the test statistic less likely to exceed 1.65. Figure 9 in Appendix B displays the standard deviation of the test statistics. It is comforting that the test is conservative in such scenarios because these localized eigenvectors \tilde{x} are often particularly troubling artifacts of noise. For example, the consistency result in Section 4.2 requires an additional step to EigCV that discards localized eigenvectors. The current simulation suggests that the additional step is a technical requirement. For this reason, we do not include the additional step in EigCV.

Appendix B.2.2 repeats these figures with folds = 10. Increasing the number of folds makes the T_3 and T_4 even more conservative, while making T_2 more powerful. This happens because the variation in T_ℓ comes from both the original data A and the edge splitting. By increasing the number of folds, the second source of variation diminishes while not disrupting the expectation of T_ℓ .

6 Comparing to other approaches

This section compares the proposed method (EigCV) with some existing graph dimensionality estimators using both simulated and real graph data. Throughout, we set the graph splitting probability ε to 0.05, set the significance level cut-off at $\alpha = 0.05$, and folds = 10.

We compare EigCV to (1) BHMC, a spectral method based on the Bethe-Hessian matrix with correction [Le and Levina, 2019]; (2) LR, a likelihood ratio method adapting a Bayesian information criterion [Wang and Bickel, 2017]; (3) ECV, an edge cross-validation method with an area under the curve criterion [Li et al., 2020]; (4) NCV, a node cross-validation using a binomial deviance criterion [Chen and Lei, 2018]; and (5) StGoF (with $\alpha = 0.05$), a stepwise goodness-of-fit estimate [Jin et al., 2020]. We performed all computations in R. For (1)-(4), we invoked the R package `randnet`, and for (5), we implemented the original Matlab code (shared by the authors) in R.¹

¹The R code is also available at <https://github.com/RoheLab/gdim>.

6.1 Numerical experiments

This section presents several simulation studies that compare our method with other approaches to graph dimensionality. We sampled random graphs with $n = 2,000$ nodes and $k = 10$ blocks from the Degree-Corrected Stochastic Blockmodel (DCSBM). Specifically, for any $i, j = 1, 2, \dots, n$,

$$A_{ij} \stackrel{\text{ind.}}{\sim} \text{Bernoulli}(\theta_i \theta_j B_{z(i)z(j)}),$$

where $z(i) \in \{1, 2, \dots, k\}$ is the block membership of node i , and $B \in \mathbb{R}^{k \times k}$ is the block connectivity matrix, with $B_{ii} = 0.28$ and $B_{ij} = 0.08$ for $i, j = 1, 2, \dots, k$, and $\theta_i > 0$ is the degree parameters of node i . We investigated the effects of degree heterogeneity by drawing θ_i 's from three distributions (before scaling to unit sum): (i) a point mass distribution, (ii) an Exponential distribution with rate 5, (iii) a Pareto distribution with location parameter 0.5 and dispersion parameter 5. From (i) to (iii), the node degrees become more heterogeneous. Finally, to examine the effects of sparsity, we chose the expected average node degree in $\{25, 30, \dots, 60\}$. For each simulation setting, we evaluated all methods 100 times.

Figure 6 displays the accuracy of all graph dimensionality methods. Here, the accuracy is the fraction of times an estimator successfully identified the true underlying graph dimensionality (which is 10).² From the results, both BHMC and ECV offered satisfactory estimation when the graph is degree-homogeneous and the average degree becomes sufficiently large, while they were affected drastically by the existence of degree heterogeneity. The LR estimate was affected by degree heterogeneity as well (although less than BHMC or ECV) and also required a relatively large average node degree to estimate the graph dimensionality. The NCV methods failed to estimate the graph dimensionality under most settings. The StGoF estimate worked better for degree-heterogeneous graphs but required a larger average node degree for accuracy. It is also worth pointing out that the LR and StGoF methods tended to over-estimate the graph dimensionality when the average degree is large, especially for the power-law graphs (see Supporting Figure 12). Finally, our method provided a much more accurate dimensionality estimate overall, requiring smaller average node degree and allowing degree heterogeneity. In addition, our testing approach also enjoys a strong advantage of reduced computational cost. To show this, Figure 7 depicts the average runtime for each method. It can be seen that the proposed method and BHMC are faster than competing methods by several orders of magnitude. The computational complexity of each StGoF iteration (or test) is at least $O(n^2)$, regardless of whether

²Besides comparison of accuracy, we also compared the deviation of the estimation by each method, for which similar results hold consistently (see Supporting Figure 12).

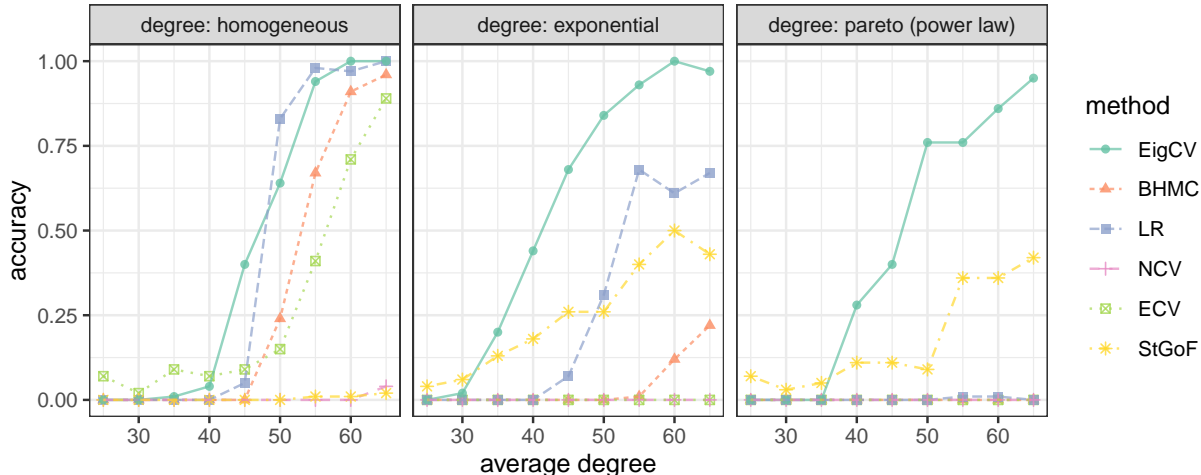


Figure 6: Comparison of accuracy for different graph dimensionality estimates under the DCSBM. The panel strips on the top indicate the node degree distribution used. Within each panel, each colored line depicts the relative error of each estimation method as the average node degree increases. Each point on the lines are averaged across 100 repeated experiments.

the graph is sparse or not. Consequently, StGoF requires the longest runtime.

6.2 Email network

A real data network was generated using email data within a large European research institution, with each node representing one of the 1005 core members [Leskovec et al., 2007]. There is an edge from node i to node j , if i sent at least one email to j . The dataset also contains 42 “ground-truth” community memberships of the nodes. That is, each individual belongs to exactly one of 42 departments at the research institute. For simplicity, we removed the 14 small departments that consist of less than 10 members (see Supporting Table 2 for similar results without the filter). This resulted in a directed and unweighted network with a total of 936 nodes from 28 communities.

We applied the graph dimensionality methods to estimate the number of clusters in the network. For the randomized methods (including ECV, NCV, and our proposed method), we ran them 25 times and report the mean and standard deviation of the estimates. For the methods that report a p -value (including StGoF and our proposed method), we use a significance level of $\alpha = 0.01$, followed by a multiplicity correction using the procedure of Benjamini and Hochberg [1995]. We set $k_{\max} = 50$. Finally, we chose the splitting probability to be 0.05, as the network is sparse with an average node degree of 23.5. Table

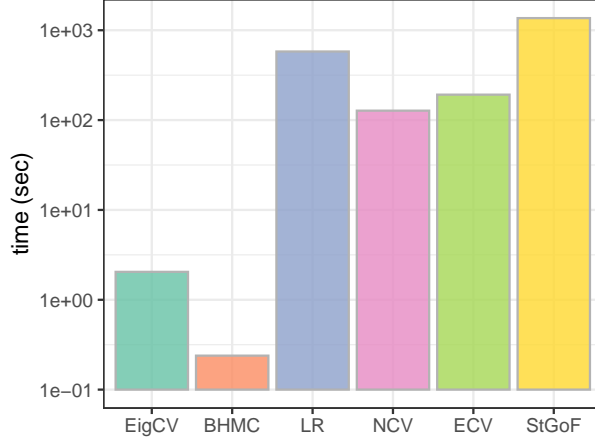


Figure 7: Comparison of runtime for the different graph dimensionality methods. Each colored bar indicates the runtime of applying each method on a DCSBM graph with 2000 nodes and 10 blocks. The maximum graph dimensionality is set to 15 for all methods. The runtime was averaged across 100 repeated experiments.

1 lists the inferences made by each method. As shown, our method provided an estimate that is close to the true number of departments within the institute. BHMC, LR, NCV, and ECV all estimated small numbers of clusters, while StGoF went significantly larger (≥ 50). These observations were consistent with the simulation results (see Supporting Figure 12). Among all the others, only the proposed method provided a close estimate (≈ 28) to the true number of departments. Similarly to the simulation results, the BHMC method and our method are more computationally efficient, with much shorter runtime than the others.

Table 1: Comparison of graph dimensionality estimates using the email network among members in a large European research institution. Each members belongs to one of 28 departments.

Method	Estimate (mean)	Runtime (second)
EigCV	28.3	0.68
BHMC	14	0.02
LR	17	85.19
NCV	6.5	204.97
ECV	16.5	41.07
StGoF	≥ 50	397.47

7 Discussion

In this paper, we proposed a new way to estimate the number of latent dimensions in a graph k using the concept of cross-validated eigenvalues. Through edge splitting and thanks to a simple central limit theorem, the estimation of cross-validated eigenvalues is efficient for very large graphs. The paper also provides theoretical justification showing that the estimator is consistent. Our simulations and empirical data application validate the theory and further demonstrate the efficacy of the proposed method.

In addition to being quickly computable, a key advantage of cross-validated eigenvalues is our rigorous understanding of their behavior outside of the asymptotic setting where all k dimensions can be estimated. Theorem 3.1 encodes this rigorous understanding into a p -value. This theorem requires very little of the population matrix P ; it does not presume that it is from a Degree-Corrected Stochastic Blockmodel, nor does it presume the actual rank of P or the order of the eigenvalue being tested. Of course, this level of ease and generality comes with a price. In particular, we only get to compute the eigenvectors with $1 - \varepsilon$ fraction of the edges. The natural possibility is to estimate k with a fraction of the edges and then recompute the eigenvectors with the full graph. Going forward, we hope others will join us in crafting new estimators for $\lambda_P(\hat{x}_j)$ that do not require leaving out edges.

Acknowledgments

This research is partially supported by the National Science Foundation under Grant DMS-1612456 (to K.R.), DMS-1916378 (to S.R. and K.R.), CCF-1740707 (TRIPODS Phase I) and DMS-2023239 (TRIPODS Phase II), and the Army Research Office under Grant W911NF-15-1-0423 (to K.R.). We thank Sündüz Keleş, Po-Ling Loh, Michael A Newton, Kris Sankaran, Muzhe Zeng, Alex Hayes, E Auden Krauska, Sijia Fang, and Jitian Zhao for all the helpful discussions.

Appendices

A Technical proofs

A.1 Proof of Proposition 2.1

Proof. Let $\hat{X} \in \mathbb{R}^{n \times q}$ contain the leading q sample eigenvectors $\hat{x}_1, \dots, \hat{x}_q$ in its columns. We aim to show that

$$\min_{\Gamma \text{ is diagonal}} \|P - \hat{X}\Gamma\hat{X}^T\|_F$$

contains $\lambda_P(\hat{x}_1), \dots, \lambda_P(\hat{x}_q)$ down the diagonal.

Using the symmetry of P and the cyclic property of the trace, we obtain

$$\begin{aligned} \|P - \hat{X}\Gamma\hat{X}^T\|_F^2 &= \text{tr}(P^2) + \text{tr}(\hat{X}\Gamma^2\hat{X}^T) - 2\text{tr}(P\hat{X}\Gamma\hat{X}^T) \\ &= \text{tr}(P^2) + \text{tr}(\Gamma^2) - 2\text{tr}(\hat{X}^T P \hat{X} \Gamma). \end{aligned}$$

Taking a derivative with respect to the diagonal of Γ and setting equal to zero gives

$$\Gamma = \text{diag}(\hat{X}^T P \hat{X})$$

which contains $\lambda_P(\hat{x}_1), \dots, \lambda_P(\hat{x}_q)$ down the diagonal. \square

A.2 Proof of Theorem 3.1

Proof. We will use Lyapunov's CLT for triangular arrays with fourth moment condition (see, e.g., [Durrett \[2019, Exercise 3.4.12\]](#)). Recall that B_{ij} is Poisson with mean Q_{ij} . Its mean and variance are Q_{ij} , while its central fourth moment is $Q_{ij}(1 + 3Q_{ij}) \leq 4Q_{ij}$ under the assumption $Q_{ij} \leq 1$. Note that $\sigma^2 = 2 \sum_{i < j} (x_i x_j)^2 Q_{ij} - \sum_{i=j} (x_i x_j)^2 Q_{ij} = \sum_{i < j} (2 - \mathbf{1}\{i = j\})^2 (x_i x_j)^2 Q_{ij}$. To use Lyapunov's CLT, taking into account the symmetry of B , we show that the following ratio converges to zero:

$$\begin{aligned} & \frac{\sum_{i < j} \mathbb{E} |(2 - \mathbf{1}\{i = j\}) x_i x_j (B_{ij} - Q_{ij})|^4}{\sigma^4} \\ & \leq \frac{\sum_{i < j} (2 - \mathbf{1}\{i = j\})^4 (x_i x_j)^4 (4Q_{ij})}{\sigma^4} \\ & \leq \frac{16 \|x\|_\infty^4 \sum_{i < j} (2 - \mathbf{1}\{i = j\})^2 (x_i x_j)^2 Q_{ij}}{\sigma^4} \\ & = \frac{16 \|x\|_\infty^4}{\sigma^2} \\ & = o(1), \end{aligned} \tag{13}$$

where we used the bound on the fourth moment in the first inequality and the delocalization condition on the last line. This shows that

$$\frac{\lambda_B(x) - \lambda_Q(x)}{\sigma^2} \Rightarrow N(0, 1). \quad (14)$$

Via Slutsky's Lemma, we can multiply the ratio in Equation (14) by any sequence that converges to one in probability and the result still holds. The proof is then concluded by showing that $\sigma/\hat{\sigma}$ converges to one in probability. Indeed, we have

$$\begin{aligned} \text{Var} \left(\frac{\hat{\sigma}^2}{\sigma^2} \right) &= \frac{\text{Var}[(x^2)^\top B x^2 - (x^2)^\top \text{diag}(B)x^2]}{\sigma^4} \\ &= \frac{\text{Var}[\sum_{i \leq j} (2 - \mathbf{1}\{i = j\})^2 (x_i x_j)^2 B_{ij}]}{\sigma^4} \\ &= \frac{\sum_{i \leq j} (2 - \mathbf{1}\{i = j\})^4 (x_i x_j)^4 Q_{ij}}{\sigma^4}, \end{aligned}$$

which is Equation (13) up to a factor of 4 and thus $o(1)$. So, by Chebyshev's inequality, $\hat{\sigma}^2/\sigma^2$ converges in probability to its expectation. Note that $\mathbb{E}(\hat{\sigma}^2/\sigma^2) = 1$ and that taking the inverse and the square root is continuous transformation. So, the ratio $\sigma/\hat{\sigma}$ converges in probability to one. \square

A.2.1 Corollary A.1

The following corollary gives a sufficient condition for $\|x\|_\infty^2 = o(\sigma)$ to hold in terms of m and the expected number of edges in B .

Corollary A.1. *Using the setting of Theorem 3.1, let $\pi \in \mathbb{R}^n$ be a probability distribution on the nodes with π_i proportional to a node's expected degree. Define $\langle \pi, x^2 \rangle$ be the expected value of x_I^2 for I drawn from π and define $m = 2^{-1} \sum_i d_i$ as the expected total number of edges. If Q is positive semi-definite and*

$$\frac{\|x\|_\infty^2}{\langle \pi, x^2 \rangle} = o(\sqrt{m}),$$

then the CLT in Equation (11) holds.

Proof. The proof of Corollary A.1 follows directly from the next lemma.

Lemma A.1. *Suppose $Q \in \mathbb{R}_+^{n \times n}$ is positive semi-definite. Define $d = Q\mathbf{1}_n \in \mathbb{R}^n$ to be the*

expected degrees of the nodes $1, \dots, n$, where $\mathbf{1}_n \in \mathbb{R}^n$ is a vector of 1's. Then,

$$\sigma^2 = 2(x^2)^\top Q x^2 - (x^2)^\top \text{diag}(Q) x^2 \geq \frac{\langle d, x^2 \rangle^2}{\sum_i d_i}.$$

Proof. Define $y = x^2$, $\theta = d^{1/2}$, $\Theta = \text{diag}(\theta) \in \mathbb{R}^{n \times n}$, $y_\theta = \Theta y$, and $\mathcal{L} = \Theta^{-1} Q \Theta^{-1}$. Because the elements of θ are non-negative, \mathcal{L} is non-negative definite.

The first part of the proof is to show that $\mathcal{L}\theta = \theta$. This is because $\Theta^{-2}Q$ is a Markov transition matrix. So,

$$\Theta^{-2}Q\mathbf{1}_n = \mathbf{1}_n \implies \Theta^{-1}Q\Theta^{-1}\Theta\mathbf{1}_n = \Theta\mathbf{1}_n$$

and this implies that $\mathcal{L}\theta = \theta$. So, by the Perron-Frobenius Theorem, θ is the leading eigenvector of \mathcal{L} with eigenvalue 1.

Let \mathcal{L} have eigenvectors and eigenvalues $(\phi_1, \lambda_1), \dots, (\phi_n, \lambda_n)$, where $\phi_1 = \theta / \|\theta\|_2$, $\lambda_1 = 1$ and $0 \leq \lambda_j \leq 1$ for $j \neq 1$. Then,

$$y^\top Q y = y_\theta^\top \mathcal{L} y_\theta = \sum_{\ell=1}^n \lambda_\ell \langle \phi_\ell, y_\theta \rangle^2.$$

Keeping only the first order term on the right-hand side, we have

$$y^\top Q y \geq \lambda_1 \langle \phi_1, y_\theta \rangle^2 = \frac{\langle d, x^2 \rangle^2}{\sum_i d_i}.$$

The desired result follows from the fact that $\sigma^2 = y^\top Q y + y^\top (Q - \text{diag}(Q)) y \geq y^\top Q y$, since y and Q have non-negative entries. \square

Applying the bound in the lemma to the delocalization condition and rearranging gives the claim. \square

A.3 Proof of consistency

This section details the proof of Theorem 4.1.

Notation We use the notation $[n]$ to refer to $\{1, 2, \dots, n\}$. For any real numbers $a, b \in \mathbb{R}$, we denote $a \vee b = \max\{a, b\}$ and $a \wedge b = \min\{a, b\}$. For non-negative a_n and b_n that depend on n , we write $a_n \lesssim b_n$ to mean $a_n \leq C b_n$ for some constant $C > 0$, and similarly for $a_n \gtrsim b_n$. Also we write $a_n = O(b_n)$ to mean $a_n \leq C b_n$ for some constant $C > 0$. The matrix spectral

norm is $\|M\| = \max_{\|x\|_2=1} \|Mx\|_2$, the matrix max-norm is $\|M\|_{\max} = \max_{i,j} |M_{ij}|$, and the matrix $2 \rightarrow \infty$ norm is $\|M\|_{2,\infty} = \max_i \|M_{i,\cdot}\|_2$.

A.3.1 Modified algorithm

Algorithm 3 is used in the consistency result.

Input: Adjacency matrix $A \in \mathbb{N}^{n \times n}$, edge splitting probability $\varepsilon \in (0, 1)$

Procedure EigCV'(A, ε, k_{\max}):

1. Obtain $\tilde{A}, \tilde{A}_{\text{test}} \leftarrow \text{ES}(A, \varepsilon)$ from splitting A and set $S = \emptyset$. // Algorithm 1

2. **for** $k = 2, \dots, k_{\max}$ **do**

a - compute $\tilde{\lambda}_{\text{test}}(\tilde{x}_k) = \tilde{x}_k^T \tilde{A}_{\text{test}} \tilde{x}_k$ and $\tilde{\sigma}_k = \sqrt{\frac{\varepsilon}{1-\varepsilon} (\tilde{x}_k^2)^T (2\tilde{A} - \text{diag}(\tilde{A})) \tilde{x}_k^2}$

b - if

$$\|\tilde{x}_k\|_{\infty}^2 \leq \min \left\{ \frac{\tilde{\sigma}_k^2}{\log^2 n}, \frac{\log n}{n} \right\},$$

add k to S and compute

$$T_k = \frac{\tilde{\lambda}_{\text{test}}(\tilde{x}_k)}{\tilde{\sigma}_k}.$$

Output: The graph dimensionality estimate: $\hat{K} = |\{T_k \geq \sqrt{n \log n} : k \in S\}|$.

Algorithm 3: Modified eigenvalue cross-validation

A.3.2 Some concentration bounds

We will need several concentration bounds for Poisson random variables. We derive them from standard results.

We begin with a simple moment growth bound.

Lemma A.2 (Poisson moment growth). *Let Z be a Poisson random variable with mean $\mu \leq 1$. There exists a universal constant $C > 0$ such that, for all integers $p \geq 2$,*

$$\mathbb{E}[|Z - \mu|^p] \leq C\mu \frac{p!}{2} \left(\frac{e}{2}\right)^{p-2}.$$

Proof. We show that

$$\mathbb{E}[|Z - \mu|^p] \leq C'\mu \left(\frac{p}{2}\right)^p, \tag{15}$$

for some constant $C' > 0$. The claim then follows from Stirling's formula in the form

$$\sqrt{2\pi p}^{p+1/2} e^{-p} \leq p!, \quad \forall p \geq 1.$$

By the definition of the Poisson distribution and using the fact that $0 \leq \mu \leq 1$ by assumption, we have

$$\begin{aligned} \mathbb{E}[|Z - \mu|^p] &= \sum_{z \geq 0} |z - \mu|^p e^{-\mu} \frac{\mu^z}{z!} \\ &= |\mu|^p e^{-\mu} + |1 - \mu|^p e^{-\mu} \mu + \sum_{z \geq 2} |z - \mu|^p e^{-\mu} \frac{\mu^z}{z!} \\ &\leq 2\mu + \mu^2 e \left\{ \sum_{z \geq 0} z^p \frac{e^{-1}}{z!} \right\}. \end{aligned}$$

The term in curly brackets on the last line is the p -th moment of a Poisson random variable with mean 1, which is $\leq C'' \left(\frac{p}{2}\right)^p$ for some constant $C'' > 0$ by [Ahle \[2021, Theorem 1\]](#). Eq. (15) follows. \square

The moment growth bound implies concentration for linear combinations of independent Poisson random variables.

Lemma A.3 (General Bernstein for Poisson variables). *Let Z_1, \dots, Z_m be independent Poisson random variables with respective means $\mu_1, \dots, \mu_m \leq 1$. For any $\boldsymbol{\alpha} = (\alpha_1, \dots, \alpha_m) \in \mathbb{R}^m$ and $t > 0$,*

$$\mathbb{P} \left[\sum_{i=1}^m \alpha_i (Z_i - \mu_i) \geq t \right] \leq \exp \left(- \frac{t^2}{C' \mu_{\max} \|\boldsymbol{\alpha}\|_2^2 + C'' \|\boldsymbol{\alpha}\|_{\infty} t} \right),$$

where $\mu_{\max} = \max_i \mu_i$ and $C', C'' > 0$ are universal constants.

Proof. We use [Boucheron et al. \[2013, Corollary 2.11\]](#). Observe that

$$\sum_{i=1}^m \mathbb{E}[\alpha_i (Z_i - \mu_i)^2] = \sum_{i=1}^m \alpha_i^2 \mu_i \leq \mu_{\max} \|\boldsymbol{\alpha}\|_2^2.$$

Moreover, by Lemma A.2 and Stirling's formula,

$$\begin{aligned}
\sum_{i=1}^m \mathbb{E}[\alpha_i^p (Z_i - \mu_i)_+^p] &\leq \sum_{i=1}^m \alpha_i^p C \mu_i \frac{p!}{2} \left(\frac{e}{2}\right)^{p-2} \\
&\leq C \mu_{\max} \|\boldsymbol{\alpha}\|_2^2 \frac{p!}{2} \left(\frac{e}{2} \|\boldsymbol{\alpha}\|_\infty\right)^{p-2} \\
&\leq \frac{p!}{2} v \left(\frac{e}{2} \|\boldsymbol{\alpha}\|_\infty\right)^{p-2},
\end{aligned}$$

where we define

$$v := \max\{1, C\} \mu_{\max} \|\boldsymbol{\alpha}\|_2^2.$$

The claim then follows from Boucheron et al. [2013, Corollary 2.11]. \square

The moment growth bound also implies spectral norm concentration.

Lemma A.4 (Spectral norm of Poisson graph). *Suppose $B \in \mathbb{R}^{n \times n}$ is the adjacency matrix of a Poisson graph with mean matrix Q satisfying $Q_{ij} \leq 1$ for all i, j . Let $q_{\max} = \max_{i,j} Q_{ij}$ and assume that $nq_{\max} \geq c_0 \log^{\xi_0} n$ for some $\xi_0 > 2$. Then, for any $\delta > 0$, there exists a constant $C''' > 0$ such that*

$$\|B - Q\| \leq C''' \sqrt{nq_{\max} \log n},$$

with probability at least $1 - n^{-\delta}$.

Proof. We use Tropp [2012, Theorem 6.2]. We first rewrite the matrix as a finite sum of independent symmetric random matrices

$$B - Q = \sum_{i=1}^n \sum_{j=i}^n (B_{ij} - Q_{ij}) E^{i,j},$$

where $E^{i,j} \in \mathbb{R}^{n \times n}$ with $E_{ij}^{i,j} = E_{ji}^{i,j} = 1$ and 0 elsewhere.

Observe that, for $i \neq j$,

$$(E^{i,j})^p = \begin{cases} E^{i,i} + E^{j,j} & \text{if } p = 2, 4, \dots \\ E^{i,j} & \text{if } p = 3, 5, \dots \end{cases}$$

while, if $i = j$,

$$(E^{i,i})^p = E^{i,i}, \quad p \geq 2.$$

Let $X^{i,j} := (B_{ij} - Q_{ij})E^{i,j}$. Then $\mathbb{E}X^{i,j} = 0$. Moreover, for $i \neq j$ and $p = 2, 4, \dots$, we have

$$\mathbb{E}(X^{i,j})^p = \mathbb{E}(B_{ij} - Q_{ij})^p (E^{i,i} + E^{j,j}) \preceq Cq_{\max} \frac{p!}{2} \left(\frac{e}{2}\right)^{p-2} (E^{i,i} + E^{j,j}),$$

by Lemma A.2. Similarly, for $i \neq j$ and $p = 3, 5, \dots$,

$$\mathbb{E}(X^{i,j})^p = \mathbb{E}(B_{ij} - Q_{ij})^p E^{i,j} \preceq Cq_{\max} \frac{p!}{2} \left(\frac{e}{2}\right)^{p-2} (E^{i,i} + E^{j,j}),$$

where we used the fact that the matrix $\begin{pmatrix} 1 & \alpha \\ \alpha & 1 \end{pmatrix}$ has eigenvalues $1 + \alpha, 1 - \alpha \geq 0$ when $|\alpha| \leq 1$. When $i = j$,

$$\mathbb{E}(X^{i,i})^p = \mathbb{E}(B_{ii} - Q_{ii})^p E^{i,i} \preceq Cq_{\max} \frac{p!}{2} \left(\frac{e}{2}\right)^{p-2} (2E^{i,i}).$$

Define

$$(\Sigma^2)^{i,j} := Cq_{\max}(E^{i,i} + E^{j,j}).$$

and

$$\sigma^2 = \left\| \sum_{i=1}^n \sum_{j=i}^n (\Sigma^2)^{i,j} \right\| = \left\| Cq_{\max} \sum_{i=1}^n \sum_{j=i}^n (E^{i,i} + E^{j,j}) \right\| \leq 2Cq_{\max}n,$$

where the inequality holds since $\sum_{i=1}^n \sum_{j=i}^n (E^{i,i} + E^{j,j})$ is a diagonal matrix with maximum entry $2n$. Then, by Tropp [2012, Theorem 6.2],

$$\begin{aligned} \mathbb{P}[\|B - Q\| \geq t] &= \mathbb{P}\left[\left\| \sum_{i=1}^n \sum_{j=i}^n X^{i,j} \right\| \geq t\right] \\ &\leq n \exp\left(\frac{-t^2/2}{\sigma^2 + (e/2)t}\right) \\ &\leq n \exp\left(\frac{-t^2/2}{2Cq_{\max}n + (e/2)t}\right). \end{aligned}$$

Taking $t = C''' \sqrt{nq_{\max} \log n}$ and using the fact that $nq_{\max} \geq c_0 \log^{\xi_0} n$, $\xi_0 > 2$, gives the result. \square

A.3.3 Key properties of sample eigenvectors

Consider the adjacency matrix A of a Poisson graph satisfying Assumptions 1 and 2. Fixing $\varepsilon \in (0, 1)$, let \tilde{A} and \tilde{A}_{test} be as in Section 3. Let $P = \rho_n P^0 = \mathbb{E}A = \sum_{j=1}^K \lambda_j x_j^{\text{T}} x_j$ with $\lambda_1 \geq \lambda_2 \geq \dots \geq \lambda_K > 0$. Let $\{\tilde{x}_l\}_{l=1}^{k_{\max}}$ be the collection of eigenvectors associated with eigenvalues $\{\tilde{\lambda}_l\}_{l=1}^{k_{\max}}$ of \tilde{A} . Without loss of generality, we assume $\tilde{\lambda}_1 \geq \tilde{\lambda}_2 \geq \dots \geq \tilde{\lambda}_{k_{\max}}$.

Define

$$\hat{U} = (\tilde{x}_1, \dots, \tilde{x}_K) \quad \text{and} \quad U = (x_1, \dots, x_K) \in \mathbb{R}^{n \times K}. \quad (16)$$

We will need the following event:

$$\mathcal{E}^0 = \left\{ \left\| \tilde{A} - (1 - \varepsilon)P \right\| \leq C''' \sqrt{n\rho_n \log n} \right\}.$$

Applying Lemma A.4 with $B := \tilde{A}$ and $Q := (1 - \varepsilon)P$ shows that \mathcal{E}^0 holds with high probability.

Concentration of signal eigenspace First, we use a version of the Davis-Kahan theorem to show that the signal sample eigenvectors are close to the signal population eigenspace.

Lemma A.5 (Signal eigenspace). *Under event \mathcal{E}^0 , there exists an orthonormal matrix $O \in \mathbb{R}^{K \times K}$ such that, for all $k \in [K]$,*

$$\|\tilde{y}_k - x_k\|_2 = O\left(\sqrt{\frac{\log n}{n\rho_n}}\right), \quad \|\tilde{x}_k - y_k\|_2 = O\left(\sqrt{\frac{\log n}{n\rho_n}}\right),$$

where

$$\tilde{y}_l = (\hat{U}O)_{\cdot l} = \left(\sum_{i=1}^K (\tilde{x}_i)_j O_{il} \right)_{j=1}^n, \quad y_l = (UO^T)_{\cdot l} = \left(\sum_{i=1}^K (x_i)_j O_{li} \right)_{j=1}^n.$$

Moreover, for all $k \in [K]$, $s \in [K]$, and $t \in [k_{\max}] \setminus [K]$,

$$\langle x_s, y_k \rangle = O_{ks}, \quad \langle \tilde{x}_t, \tilde{y}_k \rangle = 0.$$

Proof. We use the variant of the Davis-Kahan theorem in Yu et al. [2015, Theorem 2]. Under \mathcal{E}^0 , $\left\| \tilde{A} - (1 - \varepsilon)P \right\| = O(\sqrt{n\rho_n \log n})$. By Yu et al. [2015, Theorem 2], there exists an orthonormal matrix $O \in \mathbb{R}^{K \times K}$ such that, for all $l \in [K]$,

$$\|\tilde{y}_l - x_l\|_2 \leq \|\hat{U}O - U\|_{\text{F}} = O\left(\frac{\|\tilde{A} - (1 - \varepsilon)P\|}{\lambda_K}\right) = O\left(\sqrt{\frac{\log n}{n\rho_n}}\right),$$

and

$$\|\tilde{x}_l - y_l\|_2 \leq \|\hat{U} - UO^T\|_{\text{F}} = \|(\hat{U}O - U)O^T\|_{\text{F}} = \|\hat{U}O - U\|_{\text{F}} = O\left(\sqrt{\frac{\log n}{n\rho_n}}\right),$$

where we used $\lambda_K \geq \psi_1^{-1} \psi_1' n \rho_n$, which holds under Assumption 1.

By the orthonormality of $\{x_l\}_l$ and $\{\tilde{x}_l\}_l$, we have for $s \in [K]$,

$$\langle x_s, y_k \rangle = \sum_{l=1}^n (x_s)_l \left(\sum_{i=1}^K (x_i)_l O_{ki} \right) = \sum_{i=1}^K \left(\sum_{l=1}^n (x_s)_l (x_i)_l \right) O_{ki} = O_{ks},$$

and for $t \in [k_{\max}] \setminus [K]$,

$$\langle \tilde{x}_t, \tilde{y}_k \rangle = \sum_{l=1}^n (\tilde{x}_t)_l \left(\sum_{i=1}^K (\tilde{x}_i)_l O_{ik} \right) = \sum_{i=1}^K O_{ik} \left(\sum_{l=1}^n (\tilde{x}_t)_l (\tilde{x}_i)_l \right) = \sum_{i=1}^K O_{ik} \mathbf{1}_{\{i=t\}} = 0.$$

□

Bounds on population quantities The previous lemma implies bounds on the population quantity of interest, $\lambda_P(\tilde{x}_l)$.

Lemma A.6 (Bounding $\lambda_P(\tilde{x}_l)$). *Under event \mathcal{E}^0 ,*

$$\begin{aligned} \tilde{x}_l^\top P \tilde{x}_l &\gtrsim n \rho_n, & \forall l \in [K], \\ \tilde{x}_l^\top P \tilde{x}_l &\lesssim \log n, & \forall l \in [k_{\max}] \setminus [K]. \end{aligned}$$

Proof. For $s \in [K]$, expanding \tilde{x}_s over an orthonormal basis including $\{x_l\}_{l \in K}$, we get

$$\begin{aligned} \tilde{x}_s^\top P \tilde{x}_s &= \sum_{k=1}^K \lambda_k \langle \tilde{x}_s, x_k \rangle^2 \\ &= \sum_{k=1}^K \lambda_k \left[\langle x_k, y_s \rangle^2 - \langle x_k, y_s - \tilde{x}_s \rangle \langle x_k, \tilde{x}_s + y_s \rangle \right] \\ &\geq \sum_{k=1}^K \lambda_k O_{sk}^2 - \sum_{k=1}^K \lambda_k \|y_s - \tilde{x}_s\|_2 \|x_k\|_2^2 (\|\tilde{x}_s\|_2 + \|y_s\|_2) \end{aligned} \quad (17)$$

$$\begin{aligned} &\geq \psi_1^{-1} \psi_1' n \rho_n - O \left(2K n \rho_n \sqrt{\frac{\log n}{n \rho_n}} \right) \\ &\gtrsim n \rho_n \end{aligned} \quad (18)$$

where inequality (17) follows from Cauchy–Schwarz, the triangle inequality and $\langle x_k, y_s \rangle^2 = O_{sk}$ by Lemma A.5. Inequality (18) holds since $\sum_{k=1}^K O_{sk}^2 = 1$, $\psi_1^{-1} \psi_1' n \rho_n \leq \lambda_k \leq n \rho_n$ by Assumption 1, $\|\tilde{x}_s - y_s\|_2 = O \left(\sqrt{\frac{\log n}{n \rho_n}} \right)$ by Lemma A.5 and $\|\tilde{x}_k\|_2 = \|x_k\|_2 = \|y_s\|_2 = 1$.

For $t \in [k_{\max}] \setminus [K]$,

$$\begin{aligned}
\tilde{x}_t^\top P \tilde{x}_t &= \sum_{k=1}^K \lambda_k \langle \tilde{x}_t, x_k \rangle^2 \\
&= \sum_{k=1}^K \lambda_k \langle \tilde{x}_t, x_k - \tilde{y}_k + \tilde{y}_k \rangle^2 \\
&= \sum_{k=1}^K \lambda_k [\langle \tilde{x}_t, x_k - \tilde{y}_k \rangle + \langle \tilde{x}_t, \tilde{y}_k \rangle]^2 \\
&= \sum_{k=1}^K \lambda_k \langle \tilde{x}_t, x_k - \tilde{y}_k \rangle^2 \tag{19}
\end{aligned}$$

$$\leq K \lambda_1 \max_{k \in [K]} \|x_k - \tilde{y}_k\|_2^2 = O(\log n) \tag{20}$$

where equality (19) follows from $\langle \tilde{x}_t, \tilde{y}_k \rangle = 0$ by Lemma A.5. Equation (20) holds since $\|\tilde{y}_k - x_k\|_2 = O(\sqrt{\log n / n \rho_n})$ by Lemma A.5 and $\lambda_k \leq \lambda_1 \leq n \rho_n$ by Assumption 1. \square

Delocalization of signal eigenvectors To establish concentration of the estimate $\tilde{\lambda}_{\text{test}}(\tilde{x}_l)$ around $\varepsilon \lambda_P(\tilde{x}_l)$ for $l \in [K]$, we first need to show that \tilde{x}_l is delocalized. That result essentially follows from an entrywise version of Lemma A.5 based on a technical result of Abbe et al. [2020].

Lemma A.7 (Delocalization of signal sample eigenvectors). *There exist constants $\delta_1 > 0$, $C_1 > 0$ such that the event*

$$\mathcal{E}^1 = \left\{ \|\tilde{x}_l\|_\infty \leq C_1 \sqrt{\frac{\mu_0}{n}}, \forall l \in [K] \right\}$$

holds with probability at least $1 - 3n^{-\delta_1}$.

Proof. We use Abbe et al. [2020, Theorem 2.1] on \tilde{A} , which requires four conditions. We check these conditions next. First, let $\tilde{A}^* = (1 - \varepsilon)P$, $\Delta^* = \lambda_K$,

$$\kappa = \frac{\lambda_1}{\lambda_K} \leq \psi_1, \tag{21}$$

where the inequality follows from Assumption 1,

$$\varphi(x) = \frac{1}{32\psi_1} \min\{\sqrt{nx}, 1\},$$

and

$$\gamma = C''' \psi_1 (\psi'_1)^{-1} \sqrt{\frac{\log n}{n \rho_n}} \gtrsim \sqrt{\frac{\log n}{n^{1-\xi_1}}}, \quad (22)$$

where C''' is the constant in Lemma A.4 and $\psi_1, \psi'_1 > 0$, $\xi_1 \in (0, 1)$ are the constants in Assumption 1.

(A1) (*Incoherence*) By Abbe et al. [2020, Eq. (2.4)] and the remarks that follow it, the incoherence condition is satisfied provided

$$\mu(U) := \frac{n}{K} \|U\|_{2,\infty}^2 \leq \frac{n\gamma^2}{K\kappa^2}.$$

Under Assumption 2, $\mu(U) \leq \mu_0$ while (22) implies $n\gamma^2 = \Omega(\log n)$ and (21) implies $\kappa = O(1)$. Hence the condition is satisfied.

(A2) (*Row and columnwise independence*) By Lemma 3.1, \tilde{A} is the adjacency matrix of a Poisson graph with independent entries. In particular, $\{\tilde{A}_{ij} : i = m \text{ or } j = m\}$ are independent of $\{\tilde{A}_{ij} ; i \neq m, j \neq m\}$.

(A3) (*Spectral norm concentration*) As observed previously, applying Lemma A.4 with $B := \tilde{A}$, $Q := (1 - \varepsilon)P$ and $\delta > 0$ shows that the event

$$\mathcal{E}^0 = \left\{ \left\| \tilde{A} - (1 - \varepsilon)P \right\| \leq C''' \sqrt{n \rho_n \log n} \right\},$$

holds with probability $1 - n^{-\delta}$. Moreover, by the remark after Assumption 1,

$$\gamma \Delta^* = C''' \psi_1 (\psi'_1)^{-1} \sqrt{\frac{\log n}{n \rho_n}} \lambda_K \geq C''' \sqrt{n \rho_n \log n}.$$

Hence,

$$\mathbb{P} \left[\left\| \tilde{A} - \tilde{A}^* \right\| \leq \gamma \Delta^* \right] \geq 1 - n^{-\delta}.$$

Note further that, under Assumption 1, $\gamma = o(1)$, which implies

$$32\kappa \max\{\gamma, \varphi(\gamma)\} \leq 32\kappa \max\left\{\gamma, \frac{1}{32\psi_1}\right\} \leq 1,$$

for n large enough, as required in Abbe et al. [2020, Assumption (A3)], where we used (21).

(A4) (*Row concentration*) As required in Abbe et al. [2020, Assumption (A4)], the function

φ is continuous and non-decreasing on \mathbb{R}_+ with $\varphi(0) = 0$ and $\varphi(x)/x$ nonincreasing on \mathbb{R}_+ . Let $W \in \mathbb{R}^{n \times K}$. By standard norm bounds

$$\frac{1}{\sqrt{n}} \leq \frac{\|W\|_F}{\sqrt{n}\|W\|_{2,\infty}} \leq 1.$$

As a result, by definition of φ ,

$$\varphi\left(\frac{\|W\|_F}{\sqrt{n}\|W\|_{2,\infty}}\right) = \frac{1}{32\psi_1}.$$

Let

$$g = \Delta^* \|W\|_{2,\infty} \varphi\left(\frac{\|W\|_F}{\sqrt{n}\|W\|_{2,\infty}}\right) = \frac{1}{32\psi_1} \lambda_K \|W\|_{2,\infty}.$$

Fix $m \in [n]$ and $r \in [K]$. Applying Lemma A.3 on \tilde{A}_m with $\max_{ij} \mathbb{E} \tilde{A}_{ij} \leq (1 - \varepsilon)\rho_n$, there exist $c_2 > 0$, $c'_2 > 1$ such that

$$\begin{aligned} & \mathbb{P}\left(\left|\sum_{i \in [n]} (\tilde{A}_{mi} - \tilde{Q}_{mi}) W_{ir}\right| \geq g/\sqrt{K}\right) \\ & \leq 2 \exp\left(-\frac{g^2/K}{C'(1 - \varepsilon)\rho_n \|W_{\cdot r}\|_2^2 + C'' \|W_{\cdot r}\|_\infty g/\sqrt{K}}\right) \\ & = 2 \exp\left(-\frac{\lambda_K^2 \|W\|_{2,\infty}^2}{32^2 \psi_1^2 K C'(1 - \varepsilon)\rho_n \|W_{\cdot r}\|_2^2 + 32\psi_1 \sqrt{K} C'' \|W_{\cdot r}\|_\infty \lambda_K \|W\|_{2,\infty}}\right) \\ & \leq 2 \exp\left(-\frac{\lambda_K^2}{32^2 \psi_1^2 K C'(1 - \varepsilon)n\rho_n + 32\psi_1 \sqrt{K} C'' \lambda_K}\right) \\ & \leq 2 \exp(-c_2 n \rho_n) \\ & \leq n^{-c'_2}, \end{aligned}$$

where C' and C'' are the constants in Lemma A.3 and we used again that, by the remark after Assumption 1, $\lambda_K \geq \psi_1^{-1} \psi'_1 n \rho_n$. In the final inequality, we use that $n \rho_n \geq c_0 \log^{\xi_0} n$, $\xi_0 > 2$ under Assumption 1. Since

$$\|(\tilde{A} - \tilde{Q})_m \cdot W\|_2 \leq \sqrt{K} \sup_r \left| \sum_{i \in [n]} (\tilde{A}_{mi} - \tilde{Q}_{mi}) W_{ir} \right|,$$

a union bound over r implies

$$\mathbb{P} \left[\left\| (\tilde{A} - \tilde{Q})_m \cdot W \right\|_2 \leq g \right] \geq 1 - Kn^{-c'_2}.$$

Recall the definition of \hat{U} and U from (16). Applying Abbe et al. [2020, Theorem 2.1] and using Abbe et al. [2020, Eq. (2.4)] again, there exists $\tilde{C} > 0$ such that

$$\begin{aligned} \max_{l \in [K]} \|\tilde{x}_l\|_\infty &\leq \left\| \hat{U} \right\|_{2,\infty} \\ &\leq \tilde{C}(2\kappa + \varphi(1)) \|U\|_{2,\infty} \\ &\leq \tilde{C} \left(2\psi_1 + \frac{1}{32\psi_1} \right) \sqrt{K} \sqrt{\frac{\mu_0}{n}}, \end{aligned}$$

with probability $1 - n^{-\delta} - 2n^{-(c'_2-1)}$, where we used Assumption 2 on the last line. Taking $C_1 = \tilde{C}(2\psi_1 + \frac{1}{32\psi_1})\sqrt{K}$ and $\delta_1 = \min\{\delta, c'_2 - 1\} > 0$ gives the claim. \square

Concentration of quadratic forms Next, we show that $\tilde{\lambda}_{\text{test}}(\tilde{x}_l)$ is concentrated around $\varepsilon\lambda_P(\tilde{x}_l)$.

Lemma A.8 (Concentration of $\tilde{\lambda}_{\text{test}}(x)$). *Let $x \in \mathbb{R}^n$ be a unit vector such that*

$$\|x\|_\infty^2 \leq \frac{\log n}{n}, \tag{23}$$

then there exists $\delta_2 > 1$ such that

$$\mathbb{P} \left[\left| \sum_{i,j} x_i x_j (\tilde{A}_{\text{test}} - \varepsilon P)_{ij} \right| \leq \sqrt{\rho_n \log n} \right] \geq 1 - n^{-\delta_2}.$$

Proof. We use Lemma A.3. From $\|x\|_2 = 1$, we get

$$\begin{aligned} &\mathbb{P} \left[\left| \sum_{i,j} x_i x_j (\tilde{A}_{\text{test}} - \varepsilon P)_{ij} \right| \geq \sqrt{\rho_n \log n} \right] \\ &\leq 2 \exp \left(- \frac{(\sqrt{\rho_n \log n})^2 / 2}{C' \varepsilon \rho_n \sum_{i,j} (x_i x_j)^2 + C'' \max_{i,j} |x_i x_j| \sqrt{\rho_n \log n}} \right) \\ &\leq 2 \exp \left(- \frac{\rho_n \log n / 2}{C' \varepsilon \rho_n + C'' \|x\|_\infty^2 \sqrt{\rho_n \log n}} \right). \end{aligned}$$

By Assumption 1, $\rho_n \gg \frac{\log n}{n}$ while $\sqrt{\rho_n \log n} = o(1)$. By (23), the denominator on the last

line is $\lesssim \rho_n$ and the claim follows. \square

We also bound the variance estimate for the signal eigenvectors.

Lemma A.9 (Bound on the variance estimate). *Under event $\mathcal{E}^0 \cap \mathcal{E}^1$, for all $l \in [K]$,*

$$\tilde{\sigma}_l^2 := \frac{\varepsilon}{1-\varepsilon} (\tilde{x}_l^2)^\top \left(2\tilde{A} - \text{diag}(\tilde{A}) \right) \tilde{x}_l^2 = \Theta(\rho_n).$$

Proof. Let $\tilde{Q} = (1-\varepsilon)P$. We first show $(\tilde{x}_l^2)^\top \tilde{A} \tilde{x}_l^2$ can be controlled via $(\tilde{x}_l^2)^\top \tilde{Q} \tilde{x}_l^2$. Indeed observe that for each $l \in [K]$

$$\begin{aligned} \left| (\tilde{x}_l^2)^\top \tilde{A} \tilde{x}_l^2 - (\tilde{x}_l^2)^\top \tilde{Q} \tilde{x}_l^2 \right| &= |(\tilde{x}_l^2)^\top (\tilde{A} - \tilde{Q}) \tilde{x}_l^2| \\ &\leq \left\| \tilde{A} - \tilde{Q} \right\| \|\tilde{x}_l^2\|_2^2 \\ &\leq \left\| \tilde{A} - \tilde{Q} \right\| \|\tilde{x}_l\|_\infty^2 \|\tilde{x}_l\|_2^2 \\ &= O\left(\sqrt{n\rho_n \log n} \cdot \frac{1}{n} \right) \\ &= O\left(\sqrt{\frac{\rho_n \log n}{n}} \right) \end{aligned}$$

where we used that $\left\| \tilde{A} - \tilde{Q} \right\| = O(\sqrt{n\rho_n \log n})$ under event \mathcal{E}^0 and $\|\tilde{x}_l^2\|_\infty = \|\tilde{x}_l\|_\infty^2 = O(\frac{1}{n})$ under \mathcal{E}^1 . Moreover, observe that $\sqrt{\rho_n \log n/n} \ll \rho_n$ since $n\rho_n \geq c_0 \log^{\xi_0} n$ under Assumption 1. So

$$\left| (\tilde{x}_l^2)^\top \tilde{A} \tilde{x}_l^2 - (\tilde{x}_l^2)^\top \tilde{Q} \tilde{x}_l^2 \right| \ll \rho_n. \quad (24)$$

To get an upper bound on $\tilde{\sigma}_l^2$, note that

$$\begin{aligned} (\tilde{x}_l^2)^\top P \tilde{x}_l^2 &\leq \lambda_1 \|\tilde{x}_l^2\|_2^2 \\ &\leq \lambda_1 \cdot \|\tilde{x}_l\|_\infty^2 \cdot \|\tilde{x}_l\|_2^2 \\ &= O\left(n\rho_n \cdot \frac{1}{n} \cdot 1 \right) \\ &= O(\rho_n), \end{aligned}$$

where we used $\lambda_1 \leq n\rho_n$ by Assumption 1. Hence, we get

$$\begin{aligned}
\tilde{\sigma}_l^2 &= \frac{\varepsilon}{1-\varepsilon} \left[2(\tilde{x}_l^2)^\top \tilde{A}\tilde{x}_l^2 - (\tilde{x}_l^2)^\top \text{diag}(\tilde{A})\tilde{x}_l^2 \right] \\
&\leq \frac{2\varepsilon}{1-\varepsilon} (\tilde{x}_l^2)^\top \tilde{A}\tilde{x}_l^2 \\
&\leq \frac{2\varepsilon}{1-\varepsilon} |(\tilde{x}_l^2)^\top \tilde{A}\tilde{x}_l^2 - (\tilde{x}_l^2)^\top \tilde{Q}\tilde{x}_l^2| + \frac{2\varepsilon}{1-\varepsilon} (\tilde{x}_l^2)^\top \tilde{Q}\tilde{x}_l^2 \\
&\leq \frac{2\varepsilon}{1-\varepsilon} |(\tilde{x}_l^2)^\top \tilde{A}\tilde{x}_l^2 - (\tilde{x}_l^2)^\top \tilde{Q}\tilde{x}_l^2| + 2\varepsilon (\tilde{x}_l^2)^\top P\tilde{x}_l^2 \\
&= O(\rho_n),
\end{aligned}$$

by (24).

In the other direction, by Cauchy-Schwarz,

$$(\tilde{x}_l^2)^\top P\tilde{x}_l^2 \geq \frac{(\tilde{x}_l^\top P\tilde{x}_l)^2}{\sum_{ij} P_{ij}} \gtrsim \frac{(n\rho_n)^2}{n^2\rho_n} \gtrsim \rho_n,$$

where the middle inequality follows from Lemma A.6. Combining with (24), we have

$$\begin{aligned}
\tilde{\sigma}_l^2 &= \frac{\varepsilon}{1-\varepsilon} \left[(\tilde{x}_l^2)^\top \tilde{A}\tilde{x}_l^2 + (\tilde{x}_l^2)^\top \left(\tilde{A} - \text{diag}(\tilde{A}) \right) \tilde{x}_l^2 \right] \\
&\geq \frac{\varepsilon}{1-\varepsilon} (\tilde{x}_l^2)^\top \tilde{A}\tilde{x}_l^2 \\
&\geq \frac{\varepsilon}{1-\varepsilon} (\tilde{x}_l^2)^\top \tilde{Q}\tilde{x}_l^2 - \frac{\varepsilon}{1-\varepsilon} \left| (\tilde{x}_l^2)^\top \tilde{A}\tilde{x}_l^2 - (\tilde{x}_l^2)^\top \tilde{Q}\tilde{x}_l^2 \right| \\
&= \varepsilon (\tilde{x}_l^2)^\top P\tilde{x}_l^2 - \frac{\varepsilon}{1-\varepsilon} \left| (\tilde{x}_l^2)^\top \tilde{A}\tilde{x}_l^2 - (\tilde{x}_l^2)^\top \tilde{Q}\tilde{x}_l^2 \right| \\
&\gtrsim \rho_n.
\end{aligned}$$

That concludes the proof. \square

A.3.4 Proof of Theorem 4.1

Now, we are ready to prove Theorem 4.1.

Proof of Theorem 4.1. By Lemmas A.4 and A.7, the event $\mathcal{E}^0 \cap \mathcal{E}^1$ holds with probability $1 - 4n^{-\delta_1}$. Under $\mathcal{E}^0 \cap \mathcal{E}^1$, which depends only on \tilde{A} , the claims in Lemmas A.5, A.6 and A.9 also hold. For the rest of the proof, we condition on $\mathcal{E}^0 \cap \mathcal{E}^1$ and use the fact that \tilde{A}_{test} is independent of \tilde{A} by Lemma 3.1.

Let $\tilde{x}_l, l \in [k_{\max}]$, be the top k_{\max} unit eigenvectors of \tilde{A} and let

$$\tilde{\sigma}_l^2 = \frac{\varepsilon}{1 - \varepsilon} (\tilde{x}_l^2)^\top \left(2\tilde{A} - \text{diag}(\tilde{A}) \right) \tilde{x}_l^2.$$

Define

$$S = \left\{ l \in [k_{\max}] : \|\tilde{x}_l\|_\infty^2 \leq \min \left\{ \frac{\tilde{\sigma}_l^2}{\log^2 n}, \frac{\log n}{n} \right\} \right\},$$

to be the subset of $[k_{\max}]$ corresponding to sufficiently delocalized eigenvectors. Recall that the test statistic associated to \tilde{x}_l is

$$T_l = \frac{\tilde{x}_l^\top \tilde{A}_{\text{test}} \tilde{x}_l}{\tilde{\sigma}_l}.$$

We say that l is rejected if

$$l \in S \quad \text{and} \quad |T_l| \geq \sqrt{n \log n} =: \tau_n.$$

No under-estimation We show that the test statistic associated with the K leading eigenvectors of \tilde{A} will reject the null hypothesis with high probability, that is,

- $[K] \subset S$; and
- $|T_l| \geq \tau_n, \forall l \in [K]$.

Fix $s \in [K]$. First, we check that $s \in S$. Under \mathcal{E}^1 , $\|\tilde{x}_s^2\|_\infty = O(1/n) \ll \log n/n$. We need to check that $\|\tilde{x}_s^2\|_\infty \leq \tilde{\sigma}_s^2 / \log^2 n$, for n sufficiently large. This follows from the fact that $\tilde{\sigma}_s^2 = \Theta(\rho_n)$ by Lemma A.9 and $\rho_n \geq c_0 n^{-1} \log^{\xi_0} n$ with $\xi_0 > 2$ under Assumption 1.

Next, we bound $|T_s|$ from below. We have, with probability $1 - n^{-\delta_2}$, where $\delta_2 > 1$ is the constant in Lemma A.8,

$$\begin{aligned} |T_s| &= \left| \frac{\tilde{x}_s^\top \tilde{A}_{\text{test}} \tilde{x}_s}{\tilde{\sigma}_s} \right| \\ &\geq \frac{\varepsilon \left| \tilde{x}_s^\top P \tilde{x}_s \right| - \left| \tilde{x}_s^\top (\tilde{A}_{\text{test}} - \varepsilon P) \tilde{x}_s \right|}{\tilde{\sigma}_s} \\ &\gtrsim \frac{\varepsilon n \rho_n - \sqrt{\rho_n \log n}}{\sqrt{\rho_n}} \\ &\gtrsim n \sqrt{\rho_n} \\ &\gg \sqrt{n \log n}, \end{aligned} \tag{25}$$

where the dominating term is controlled through $|\tilde{x}_s^\top P \tilde{x}_s| \gtrsim n \rho_n \gg \log n$ by Lemma A.6, the term $|\tilde{x}_s^\top (\tilde{A}_{\text{test}} - \varepsilon P) \tilde{x}_s|$ is bounded above by $\sqrt{\rho_n \log n} \ll \log n$ from Lemma A.8 and the denominator satisfies $\tilde{\sigma}_s^2 = \Theta(\rho_n)$ by Lemma A.9. The final bound follows from Assumption 1. By a union bound, (25) holds simultaneously for $s \in [K]$ with probability $1 - Kn^{-\delta_2}$.

No over-estimation Then, we show that the noise eigenvectors of \tilde{A} will either be too localized or the test statistic associated with them will fail to reject the null hypothesis. In other words, we show that for any $s \in S \setminus [K]$, it holds that $|T_s| < \tau_n$ with high probability.

Let $t \in S \setminus [K]$. We bound $|T_t|$ from above as follows

$$\begin{aligned} |T_t| &= \left| \frac{\tilde{x}_t^\top \tilde{A}_{\text{test}} \tilde{x}_t}{\tilde{\sigma}_t} \right| \\ &\leq \frac{\varepsilon |\tilde{x}_t^\top P \tilde{x}_t| + |\tilde{x}_t^\top (\tilde{A}_{\text{test}} - \varepsilon P) \tilde{x}_t|}{\tilde{\sigma}_t} \end{aligned} \quad (26)$$

$$\begin{aligned} &= O\left(\sqrt{\frac{n}{\log^2 n}} \cdot (\log n + \sqrt{\rho_n \log n})\right) \\ &= O(\sqrt{n}). \end{aligned} \quad (27)$$

The first term in the numerator of (26) satisfies $|\tilde{x}_t^\top P \tilde{x}_t| = O(\log n)$ by Lemma A.6 while the term $|\tilde{x}_t^\top (\tilde{A}_{\text{test}} - \varepsilon P) \tilde{x}_t|$ in (26) is bounded above by $\sqrt{\rho_n \log n} \ll \log n$ from Lemma A.8. For the denominator $\tilde{\sigma}_t$, $t \in S$ implies that $\|\tilde{x}_t^2\|_\infty \leq \tilde{\sigma}_t^2 / \log^2 n$, thus

$$\tilde{\sigma}_t^2 \geq \log^2 n \cdot \|\tilde{x}_t^2\|_\infty \geq \frac{\log^2 n}{n} \cdot n \|\tilde{x}_t^2\|_\infty \geq \frac{\log^2 n}{n} \cdot \|\tilde{x}_t\|_2^2 = \frac{\log^2 n}{n}.$$

By a union bound, (27) holds simultaneously for $t \in S \setminus [K]$ with probability at least $1 - n^{-\delta_2+1}$.

Consistency Therefore, it follows that the algorithm outputs $\hat{K} = K$ with probability tending to 1. \square

B Supporting figures and tables

B.1 Details of Degree-Corrected Stochastic Blockmodel in the introduction, Figures 1 and 2

In the introduction, the simulated graph comes from a Degree-Corrected Stochastic Blockmodel (DCSBM). See Section 6.1 for a description of this model and its parameters. In Figures 1 and 2, the DCSBM has $k = 128$ blocks. The 2,560 nodes are randomly assigned to the 128 blocks with uniform probabilities. On average, each block contains 20 nodes. The smallest block has 10 nodes and the largest block has 32. The degree parameters θ_i are distributed as Exponential($\lambda = 1$) and the B matrix is hierarchically structured. In order to specify the elements of B , let \mathbb{T} be a complete binary tree with 7 generations (i.e., $2^7 = 128$ leaves). Each leaf node is assigned to one of the $k = 128$ blocks. Define $u \wedge v \in \mathbb{T}$ as the most recent common ancestor of u and v (i.e., the node closest to the root along the shortest path between u and v). Define $g(u, v)$ as the distance in \mathbb{T} from the root to $u \wedge v$. So, if the shortest path between u and v passes through the root, then $g(u, v) = 0$. Moreover, $g(u, u) = 7$ for all leaf nodes u . Set $B_{u,v} = p2^{g(u,v)}$, where $p = .0008$ is chosen so that the average expected degree of the nodes is equal to 20.

B.2 Bernoulli vs. Poisson

B.2.1 Two clarifying figures for folds = 1

The average value of T_3 and T_4 are different under the Poisson and Bernoulli models (see Figure 5 in Section 5). To further illustrate this difference and to show that T_2 does not have the same property, Figure 8 subtracts the average value of the test statistic *under the Bernoulli model* from the corresponding average under the Poisson model. The difference appears for T_3 and T_4 , but not for T_2 . This shows that $\tilde{x}_\ell^T \tilde{A} \tilde{x}_\ell$ and $\tilde{x}_\ell^T \tilde{A}_{\text{test}} \tilde{x}_\ell$ are negatively correlated when (1) the edges are Bernoulli, (2) the graph is dense, (3) and $\ell > k$. In the two-block Stochastic Blockmodel, this negative dependence does not shift the expectation of T_2 , even for dense Bernoulli graphs.

Figure 9 displays the standard deviation for the test statistics T_2, T_3, T_4 over the 1000 replicates in the simulation. This figure is repeated with folds = 10 in Figure 11.

B.2.2 Increasing the number of folds in the Bernoulli vs. Poisson comparison

Figure 10 repeats Figure 4, but with folds = 10 instead of 1. It shows that increasing the number of folds makes T_3 and T_4 more conservative. While Theorem 3.1 shows that T_ℓ

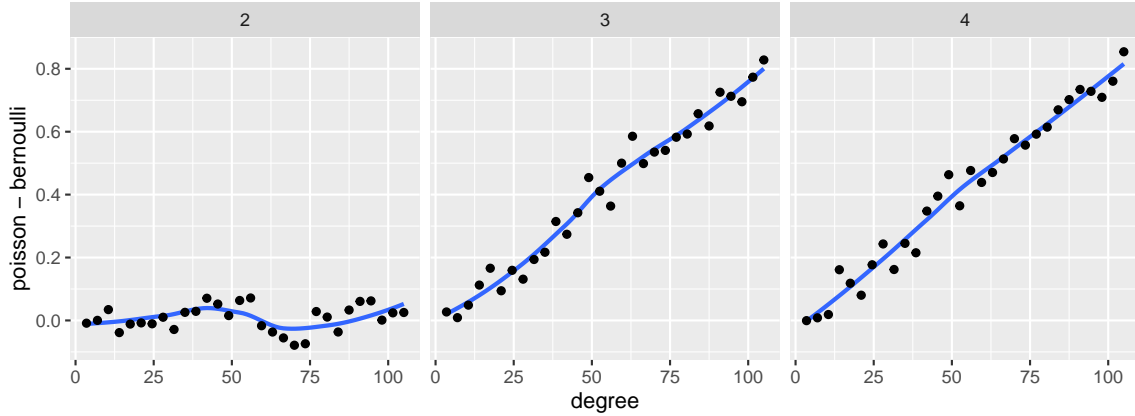


Figure 8: Each panel gives the difference between the Poisson and Bernoulli results from Figure 5. In this simulation model, there are $k = 2$ blocks in the Stochastic Blockmodel. Taken together, this suggests that the negative dependence in Bernoulli graphs between the fitting and testing adjacency matrices diminishes the expected value of T_ℓ when $\ell > k$ and the graph is more dense. However, the negative dependence does not appear to diminish the expected value of T_2 . When a test is conservative under the null, one typically suffers a reduced power under the alternative. However, this result suggests that the negative dependence require us to pay this price. The Bernoulli model makes T_3 conservative, without making T_2 less powerful.

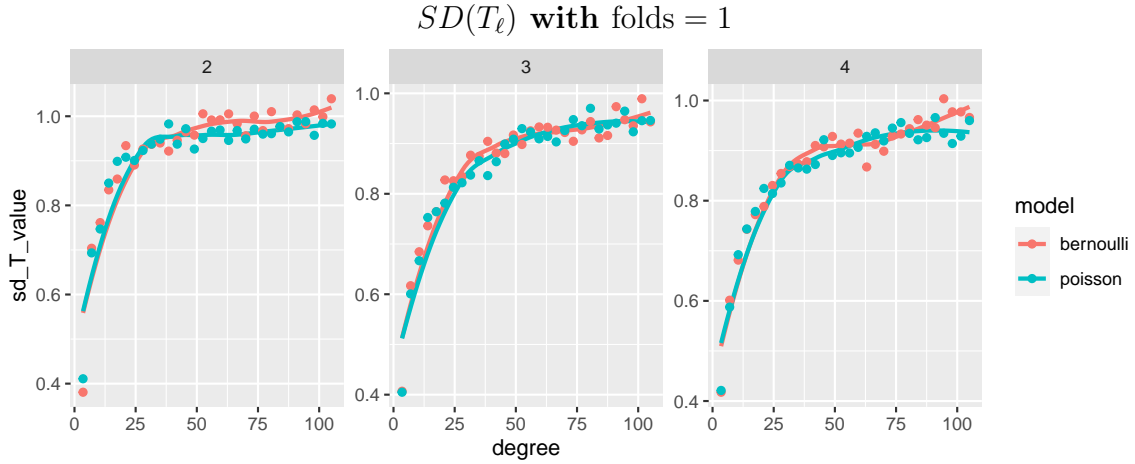


Figure 9: As discussed in Section 5, the localization of the eigenvectors on small degree graphs (on the left of each panel) makes $\tilde{\sigma}$ over estimate the standard error. This makes the standard deviation of the test statistics over the 1000 replicates smaller than 1.

is asymptotically normal with folds = 1, increasing the number of folds induces unknown dependence between the test statistics. Figure 10 suggests that even with 10 folds, the right tail of the distribution of T_3 and T_4 are well approximated by the normal distribution; this is because the bumpy line that gives $\hat{\alpha}$ is close to the points. The tests are conservative because their expectation is not zero and their variance is not one.

Figure 11 shows that increasing the number of folds dramatically reduces the variation in T_2, T_3, T_4 . This makes T_2 more powerful and T_3, T_4 more conservative.

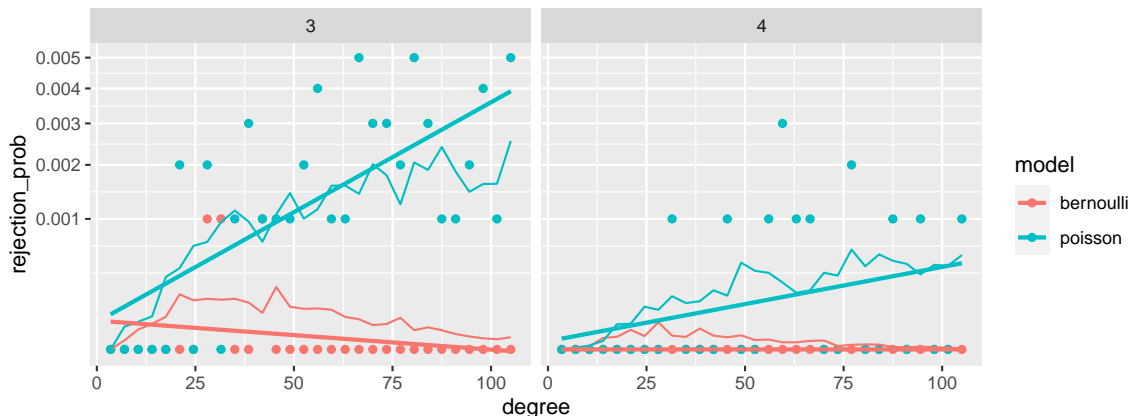


Figure 10: This is a repeat of Figure 4, but with folds = 10 instead of 1. The vertical axis gives estimates of the rejection probability for T_3 (left) and T_4 (right). Each dot give the proportion of 1000 simulations for which the test statistic exceeds 1.65. The bumpy line interpolates the values $\hat{\alpha}$, defined in Equation (12). Because there are so few rejections, particularly for T_4 , it is difficult to see whether the bumpy line is close to the points. The straight line is the ordinary least squares fit to the points. It roughly aligns with the bumpy line. This suggests that the right tails of the distributions for T_3 and T_4 are approximately normally distributed.

B.3 Comparing to other techniques

In Figure 6, we evaluated the accuracy of each method when requiring the exact recovery of k . In order to illustrate how each method either under-estimates or over-estimates k , Figure 12 displays the results in Figure 6 by the relative error for each estimate \hat{k} , which is defined as

$$\text{relative error} = \frac{\hat{k} - k^*}{k^*},$$

where $k^* = 10$ is the true k . From the simulation results, we observed that most methods under-estimate k when the average degree of the graph is smaller (i.e., sparser), except for

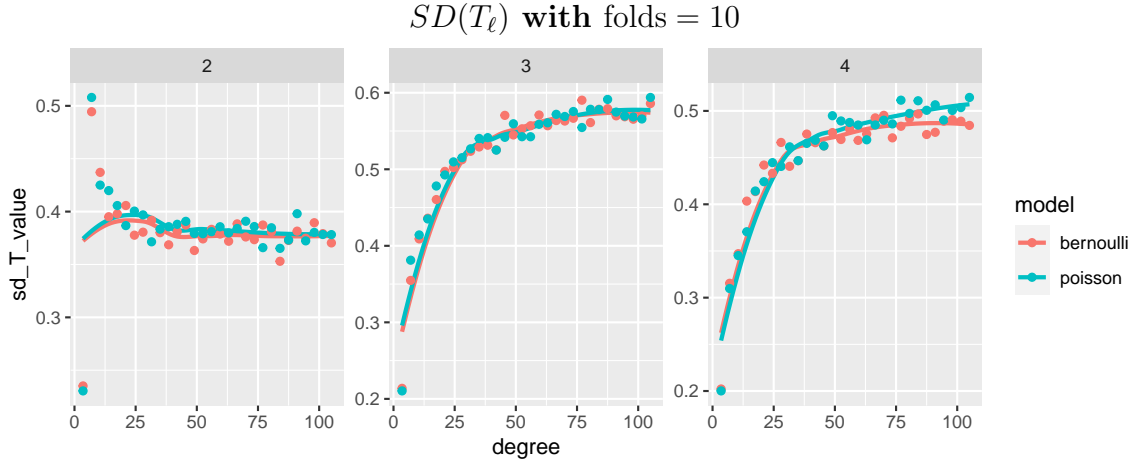


Figure 11: This is a repeat of Figure 9, but with folds = 10 instead of 1. The vertical axis gives the standard deviation of the test statistics T_2, T_3, T_4 over the 1000 replicates. Notice that they are all significantly less than one. This explains why the rejection probabilities in Figure 10 are significantly lower than .05.

StGoF which over-estimates it. In addition, from the standard deviation of the relative error, we observe that EigCV provides a more accurate and less variable estimation of k as the graph sparsity varies.

In Section 6.2, we removed the 14 small departments that consist of less than 10 members. Among these, two departments have only one members, and eight departments have less than five members. Table 2 compares six methods using this email network without filtering. We observed similarly that EigCV provided a closer estimate of k than other methods.

Table 2: Comparison of graph dimensionality estimates using the email network among members in a large European research institution. Each members belongs to one of 42 departments.

Method	Estimate (mean)	Runtime (second)
EigCV	30.56	0.81
BHMC	14.00	0.04
LR	13.00	128.17
NCV	6.96	271.15
ECV	20.08	60.13
StGoF	> 50	544.66

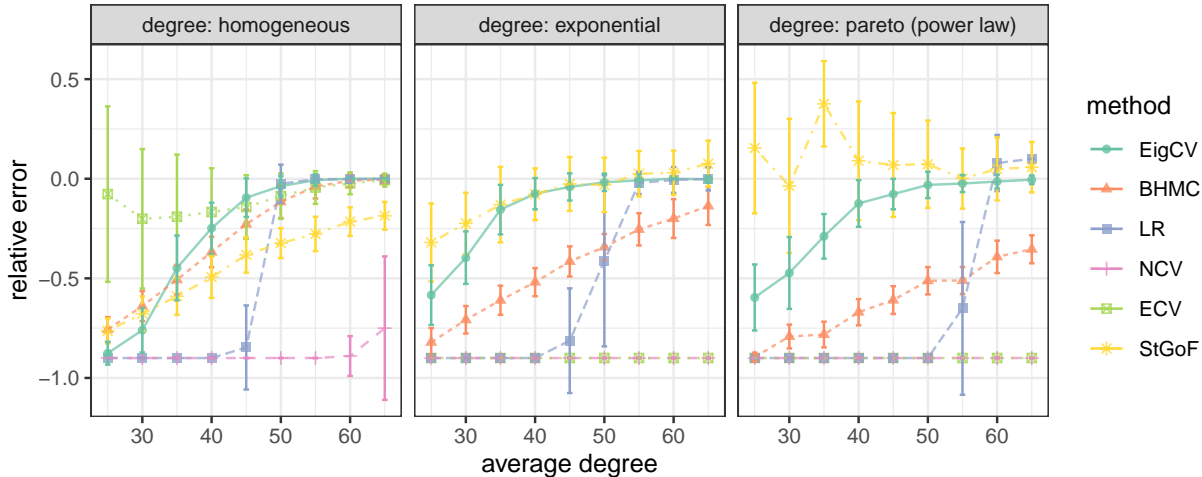


Figure 12: Comparison of relative error for different graph dimensionality estimators under the DCSBM. The panel strips on the top indicate the node degree distribution used. Within each panel, each colored line depicts the relative error of each estimation method as the average node degree increases. Each point on the lines are averaged across 100 repeated experiments. For each point, an error bar indicates the sample standard deviation of relative errors.

References

- Karim M. Abadir, Walter Distaso, and Filip Zikes. Design-free estimation of variance matrices. *Journal of Econometrics*, 181(2):165–180, August 2014. ISSN 0304-4076. doi: 10.1016/j.jeconom.2014.03.010. URL <https://www.sciencedirect.com/science/article/pii/S0304407614000591>.
- E. Abbe, A. S. Bandeira, and G. Hall. Exact Recovery in the Stochastic Block Model. *IEEE Transactions on Information Theory*, 62(1):471–487, January 2016. ISSN 1557-9654. doi: 10.1109/TIT.2015.2490670. Conference Name: IEEE Transactions on Information Theory.
- Emmanuel Abbe. Community Detection and Stochastic Block Models. *Foundations and Trends® in Communications and Information Theory*, 14(1-2):1–162, June 2018. ISSN 1567-2190, 1567-2328. doi: 10.1561/01000000067. URL <http://www.nowpublishers.com/article/Details/CIT-067>. Publisher: Now Publishers, Inc.
- Emmanuel Abbe and Colin Sandon. Community detection in general stochastic block models: fundamental limits and efficient recovery algorithms. *arXiv:1503.00609 [cs, math]*, April 2015. URL <http://arxiv.org/abs/1503.00609>. arXiv: 1503.00609.
- Emmanuel Abbe, Jianqing Fan, Kaizheng Wang, Yiqiao Zhong, et al. Entrywise eigenvector analysis of random matrices with low expected rank. *Annals of Statistics*, 48(3):1452–1474, 2020.
- Thomas D. Ahle. Sharp and Simple Bounds for the raw Moments of the Binomial and Poisson Distributions. *arXiv:2103.17027 [math, stat]*, April 2021. URL <http://arxiv.org/abs/2103.17027>. arXiv: 2103.17027.

- Edoardo Maria Airoldi, David M Blei, Stephen E Fienberg, and Eric P Xing. Mixed membership stochastic blockmodels. *Journal of machine learning research*, 2008.
- Oskari H. Ajanki, László Erdős, and Torben Krüger. Universality for general Wigner-type matrices. *Probability Theory and Related Fields*, 169(3):667–727, December 2017. ISSN 1432-2064. doi: 10.1007/s00440-016-0740-2. URL <https://doi.org/10.1007/s00440-016-0740-2>.
- David J Aldous. Exchangeability and related topics. In *École d’Été de Probabilités de Saint-Flour XIII—1983*, pages 1–198. Springer, 1985.
- Bloemendal Alex, László Erdős, Antti Knowles, Horng-Tzer Yau, and Jun Yin. Isotropic local laws for sample covariance and generalized Wigner matrices. *Electronic Journal of Probability*, 19, 2014. ISSN 1083-6489. doi: 10.1214/EJP.v19-3054. URL <http://projecteuclid.org/euclid.ejp/1465065675>. Publisher: The Institute of Mathematical Statistics and the Bernoulli Society.
- Waleed Ammar, Dirk Groeneveld, Chandra Bhagavatula, Iz Beltagy, Miles Crawford, Doug Downey, Jason Dunkelberger, Ahmed Elgohary, Sergey Feldman, Vu Ha, et al. Construction of the literature graph in semantic scholar. *arXiv preprint arXiv:1805.02262*, 2018.
- Sylvain Arlot and Alain Celisse. A survey of cross-validation procedures for model selection. *Statistics Surveys*, 4(none):40–79, January 2010. ISSN 1935-7516. doi: 10.1214/09-SS054. URL <http://projecteuclid.org/journals/statistics-surveys/volume-4/issue-none/A-survey-of-cross-validation-procedures-for-model-selection/10.1214/09-SS054.full>. Publisher: Amer. Statist. Assoc., the Bernoulli Soc., the Inst. Math. Statist., and the Statist. Soc. Canada.
- Avanti Athreya, Vince Lyzinski, David J Marchette, Carey E Priebe, Daniel L Sussman, and Minh Tang. A central limit theorem for scaled eigenvectors of random dot product graphs. *arXiv preprint arXiv:1305.7388*, 2013.
- Douglas Bates and Martin Maechler. *Matrix: Sparse and Dense Matrix Classes and Methods*, 2021. URL <https://CRAN.R-project.org/package=Matrix>. R package version 1.3-3.
- Florent Benaych-Georges, Charles Bordenave, and Antti Knowles. Largest eigenvalues of sparse inhomogeneous Erdős–Rényi graphs. *Annals of Probability*, 47(3):1653–1676, May 2019. ISSN 0091-1798, 2168-894X. doi: 10.1214/18-AOP1293. URL <http://projecteuclid.org/euclid.aop/1556784029>. Publisher: Institute of Mathematical Statistics.
- Florent Benaych-Georges, Charles Bordenave, and Antti Knowles. Spectral radii of sparse random matrices. *Annales de l’Institut Henri Poincaré, Probabilités et Statistiques*, 56(3):2141–2161, August 2020. ISSN 0246-0203. doi: 10.1214/19-AIHP1033. URL <http://projecteuclid.org/euclid.aihp/1593137322>. Publisher: Institut Henri Poincaré.
- Yoav Benjamini and Yosef Hochberg. Controlling the false discovery rate: a practical and powerful approach to multiple testing. *Journal of the Royal statistical society: series B (Methodological)*, 57(1):289–300, 1995.
- Sharmodeep Bhattacharyya and Peter J. Bickel. Subsampling bootstrap of count features of networks. *Annals of Statistics*, 43(6):2384–2411, December 2015. ISSN 0090-5364, 2168-8966. doi: 10.1214/15-AOS1338. URL <http://projecteuclid.org/euclid.aos/1444222079>. Publisher: Institute of Mathematical Statistics.

- Peter J. Bickel and Purnamrita Sarkar. Hypothesis testing for automated community detection in networks. *Journal of the Royal Statistical Society. Series B (Statistical Methodology)*, 78(1):253–273, 2016. ISSN 1369-7412. URL <http://www.jstor.org/stable/24775336>. Publisher: [Royal Statistical Society, Wiley].
- C. Bordenave, M. Lelarge, and L. Massoulié. Non-backtracking Spectrum of Random Graphs: Community Detection and Non-regular Ramanujan Graphs. In *2015 IEEE 56th Annual Symposium on Foundations of Computer Science*, pages 1347–1357, October 2015. doi: 10.1109/FOCS.2015.86. ISSN: 0272-5428.
- S. Boucheron, G. Lugosi, and P. Massart. *Concentration Inequalities: A Nonasymptotic Theory of Independence*. OUP Oxford, 2013. ISBN 978-0-19-953525-5. URL <https://books.google.com/books?id=koNqWR1uhPOC>.
- Diana Cai, Trevor Campbell, and Tamara Broderick. Edge-exchangeable graphs and sparsity. In *Proceedings of the 30th International Conference on Neural Information Processing Systems*, pages 4249–4257, 2016.
- Emmanuel J Candès and Benjamin Recht. Exact matrix completion via convex optimization. *Foundations of Computational mathematics*, 9(6):717, 2009.
- Arijit Chakrabarty, Sukrit Chakraborty, and Rajat Subhra Hazra. Eigenvalues Outside the Bulk of Inhomogeneous Erdős–Rényi Random Graphs. *Journal of Statistical Physics*, 181(5):1746–1780, December 2020. ISSN 1572-9613. doi: 10.1007/s10955-020-02644-7. URL <https://doi.org/10.1007/s10955-020-02644-7>.
- Sourav Chatterjee. Matrix estimation by Universal Singular Value Thresholding. *The Annals of Statistics*, 43(1):177–214, February 2015. ISSN 0090-5364, 2168-8966. doi: 10.1214/14-AOS1272. URL <http://projecteuclid.org/journals/annals-of-statistics/volume-43/issue-1/Matrix-estimation-by-Universal-Singular-Value-Thresholding/10.1214/14-AOS1272.full>. Publisher: Institute of Mathematical Statistics.
- Kehui Chen and Jing Lei. Network Cross-Validation for Determining the Number of Communities in Network Data. *Journal of the American Statistical Association*, 113(521):241–251, January 2018. ISSN 0162-1459. doi: 10.1080/01621459.2016.1246365. URL <https://doi.org/10.1080/01621459.2016.1246365>. Publisher: Taylor & Francis eprint: <https://doi.org/10.1080/01621459.2016.1246365>.
- Harry Crane and Walter Dempsey. Edge exchangeable models for interaction networks. *Journal of the American Statistical Association*, 113(523):1311–1326, 2018.
- Ioana Dumitriu and Yizhe Zhu. Sparse general Wigner-type matrices: Local law and eigenvector delocalization. *Journal of Mathematical Physics*, 60(2):023301, February 2019. ISSN 0022-2488. doi: 10.1063/1.5053613. URL <https://aip-scitation-org.ezproxy.library.wisc.edu/doi/full/10.1063/1.5053613>. Publisher: American Institute of Physics.
- Rick Durrett. *Probability: Theory and Examples*. Cambridge Series in Statistical and Probabilistic Mathematics. Cambridge University Press, 5 edition, 2019. doi: 10.1017/9781108591034.
- László Erdős, Antti Knowles, Horng-Tzer Yau, and Jun Yin. Spectral Statistics of Erdős–Rényi Graphs II: Eigenvalue Spacing and the Extreme Eigenvalues. *Communications in Mathematical Physics*, 314(3): 587–640, September 2012. ISSN 1432-0916. doi: 10.1007/s00220-012-1527-7. URL <https://doi.org/10.1007/s00220-012-1527-7>.

- László Erdős, Antti Knowles, Horng-Tzer Yau, and Jun Yin. The local semicircle law for a general class of random matrices. *Electronic Journal of Probability*, 18, 2013. ISSN 1083-6489. doi: 10.1214/EJP.v18-2473. URL <http://projecteuclid.org/euclid.ejp/1465064284>. Publisher: The Institute of Mathematical Statistics and the Bernoulli Society.
- Cheryl Flynn, Patrick Perry, et al. Profile likelihood biclustering. *Electronic Journal of Statistics*, 14(1): 731–768, 2020.
- Alden Green and Cosma Rohilla Shalizi. Bootstrapping Exchangeable Random Graphs. *arXiv:1711.00813 [stat]*, November 2017. URL <http://arxiv.org/abs/1711.00813>. arXiv: 1711.00813.
- Peter D Hoff, Adrian E Raftery, and Mark S Handcock. Latent space approaches to social network analysis. *Journal of the American Statistical Association*, 97(460):1090–1098, 2002.
- DN Hoover. Tail fields of partially exchangeable arrays. *Journal of Multivariate Analysis*, 31(1):160–163, 1989.
- Jong Yun Hwang, Ji Oon Lee, and Wooseok Yang. Local law and Tracy–Widom limit for sparse stochastic block models. *Bernoulli*, 26(3):2400–2435, August 2020. ISSN 1350-7265. doi: 10.3150/20-BEJ1201. URL <http://projecteuclid.org/euclid.bj/1587974546>. Publisher: Bernoulli Society for Mathematical Statistics and Probability.
- Abigail Z Jacobs and Aaron Clauset. A unified view of generative models for networks: models, methods, opportunities, and challenges. *arXiv preprint arXiv:1411.4070*, 2014.
- Jiashun Jin, Zheng Tracy Ke, Shengming Luo, and Minzhe Wang. Estimating the number of communities by Stepwise Goodness-of-fit. *arXiv:2009.09177 [math, stat]*, September 2020. URL <http://arxiv.org/abs/2009.09177>. arXiv: 2009.09177.
- Antony Joseph and Bin Yu. Impact of regularization on spectral clustering. *Annals of Statistics*, 44(4):1765–1791, August 2016. ISSN 0090-5364, 2168-8966. doi: 10.1214/16-AOS1447. URL <http://projecteuclid.org/euclid.aos/1467894715>. Publisher: Institute of Mathematical Statistics.
- Brian Karrer and M. E. J. Newman. Stochastic blockmodels and community structure in networks. *Physical Review E*, 83(1):016107, January 2011. doi: 10.1103/PhysRevE.83.016107. URL <https://link.aps.org/doi/10.1103/PhysRevE.83.016107>. Publisher: American Physical Society.
- Florent Krzakala, Cristopher Moore, Elchanan Mossel, Joe Neeman, Allan Sly, Lenka Zdeborová, and Pan Zhang. Spectral redemption in clustering sparse networks. *Proceedings of the National Academy of Sciences*, 110(52):20935–20940, December 2013. ISSN 0027-8424, 1091-6490. doi: 10.1073/pnas.1312486110. URL <http://www.pnas.org/content/110/52/20935>. Publisher: National Academy of Sciences Section: Physical Sciences.
- Clifford Lam. Nonparametric eigenvalue-regularized precision or covariance matrix estimator. *The Annals of Statistics*, 44(3):928–953, June 2016. ISSN 0090-5364, 2168-8966. doi: 10.1214/15-AOS1393. URL <http://projecteuclid.org/journals/annals-of-statistics/volume-44/issue-3/Nonparametric-eigenvalue-regularized-precision-or-covariance-matrix-estimator/10.1214/15-AOS1393.full>. Publisher: Institute of Mathematical Statistics.
- Can M. Le and Elizaveta Levina. Estimating the number of communities in networks by spectral methods. *arXiv:1507.00827 [cs, math, stat]*, November 2019. URL <http://arxiv.org/abs/1507.00827>. arXiv: 1507.00827.

- Can M. Le, Elizaveta Levina, and Roman Vershynin. Concentration and regularization of random graphs. *Random Structures & Algorithms*, 51(3):538–561, 2017. ISSN 1098-2418. doi: 10.1002/rsa.20713. URL <https://onlinelibrary.wiley.com/doi/abs/10.1002/rsa.20713>. eprint: <https://onlinelibrary.wiley.com/doi/pdf/10.1002/rsa.20713>.
- Jing Lei. A goodness-of-fit test for stochastic block models. *Annals of Statistics*, 44(1):401–424, February 2016. ISSN 0090-5364, 2168-8966. doi: 10.1214/15-AOS1370. URL <http://projecteuclid.org/euclid.aos/1452004791>. Publisher: Institute of Mathematical Statistics.
- Jure Leskovec, Jon Kleinberg, and Christos Faloutsos. Graph evolution: Densification and shrinking diameters. *ACM transactions on Knowledge Discovery from Data (TKDD)*, 1(1):2–es, 2007.
- Keith Levin and Elizaveta Levina. Bootstrapping Networks with Latent Space Structure. *arXiv:1907.10821 [math, stat]*, July 2019. URL <http://arxiv.org/abs/1907.10821>. arXiv: 1907.10821.
- Tianxi Li, Elizaveta Levina, and Ji Zhu. Network cross-validation by edge sampling. *Biometrika*, 107(2): 257–276, June 2020. ISSN 0006-3444. doi: 10.1093/biomet/asaa006. URL <https://doi.org/10.1093/biomet/asaa006>.
- Qiaohui Lin, Robert Lunde, and Purnamrita Sarkar. Higher-Order Correct Multiplier Bootstraps for Count Functionals of Networks. *arXiv:2009.06170 [math, stat]*, September 2020a. URL <http://arxiv.org/abs/2009.06170>. arXiv: 2009.06170.
- Qiaohui Lin, Robert Lunde, and Purnamrita Sarkar. On the Theoretical Properties of the Network Jackknife. In *International Conference on Machine Learning*, pages 6105–6115. PMLR, November 2020b. URL <http://proceedings.mlr.press/v119/lin20c.html>. ISSN: 2640-3498.
- Yan Liu, Zhiqiang Hou, Zhigang Yao, Zhidong Bai, Jiang Hu, and Shurong Zheng. Community Detection Based on the L_∞ convergence of eigenvectors in DCBM. *arXiv:1906.06713 [math, stat]*, June 2019. URL <http://arxiv.org/abs/1906.06713>. arXiv: 1906.06713.
- László Lovász. *Large networks and graph limits*, volume 60. American Mathematical Soc., 2012.
- Robert Lunde and Purnamrita Sarkar. Subsampling Sparse Graphons Under Minimal Assumptions. *arXiv:1907.12528 [math, stat]*, August 2019. URL <http://arxiv.org/abs/1907.12528>. arXiv: 1907.12528.
- Shujie Ma, Liangjun Su, and Yichong Zhang. Determining the Number of Communities in Degree-corrected Stochastic Block Models. *arXiv:1809.01028 [stat]*, July 2019. URL <http://arxiv.org/abs/1809.01028>. arXiv: 1809.01028.
- Elchanan Mossel, Joe Neeman, and Allan Sly. Reconstruction and estimation in the planted partition model. *Probability Theory and Related Fields*, 162(3):431–461, 2015.
- Zacharie Naulet, Daniel M. Roy, Ekansh Sharma, and Victor Veitch. Bootstrap estimators for the tail-index and for the count statistics of graphex processes. *Electronic Journal of Statistics*, 15(1):282–325, 2021. ISSN 1935-7524. doi: 10.1214/20-EJS1789. URL <http://projecteuclid.org/euclid.ejs/1609902191>. Publisher: The Institute of Mathematical Statistics and the Bernoulli Society.
- Richard R. Picard and R. Dennis Cook. Cross-Validation of Regression Models. *Journal of the American Statistical Association*, 79:575–583, 1984. ISSN 0162-1459. doi: 10.2307/2288403. URL <http://www.jstor.org/stable/2288403>. Publisher: [American Statistical Association, Taylor & Francis, Ltd.].

- Tai Qin and Karl Rohe. Regularized spectral clustering under the degree-corrected stochastic blockmodel. In *Proceedings of the 26th International Conference on Neural Information Processing Systems-Volume 2*, pages 3120–3128, 2013.
- Yixuan Qiu and Jiali Mei. *RSpectra: Solvers for Large-Scale Eigenvalue and SVD Problems*, 2019. URL <https://CRAN.R-project.org/package=RSpectra>. R package version 0.16-0.
- Karl Rohe and Muzhe Zeng. Vintage factor analysis with varimax performs statistical inference. *arXiv preprint arXiv:2004.05387*, 2020.
- Karl Rohe, Sourav Chatterjee, and Bin Yu. Spectral clustering and the high-dimensional stochastic blockmodel. *Annals of Statistics*, 39(4):1878–1915, August 2011. ISSN 0090-5364, 2168-8966. doi: 10.1214/11-AOS887. URL <http://projecteuclid.org/euclid.aos/1314190618>. Publisher: Institute of Mathematical Statistics.
- Karl Rohe, Jun Tao, Xintian Han, and Norbert Binkiewicz. A note on quickly sampling a sparse matrix with low rank expectation. *Journal of Machine Learning Research*, 19(77):1–13, 2018. URL <http://jmlr.org/papers/v19/17-128.html>.
- Tom AB Snijders and Stephen P Borgatti. Non-parametric standard errors and tests for network statistics. *Connections*, 22(2):161–170, 1999.
- Alexander Soshnikov. Universality at the Edge of the Spectrum in Wigner Random Matrices. *Communications in Mathematical Physics*, 207(3):697–733, November 1999. ISSN 1432-0916. doi: 10.1007/s002200050743. URL <https://doi.org/10.1007/s002200050743>.
- Liangjun Su, Wuyi Wang, and Yichong Zhang. Strong Consistency of Spectral Clustering for Stochastic Block Models. *arXiv:1710.06191 [stat]*, May 2019. URL <http://arxiv.org/abs/1710.06191>. arXiv: 1710.06191.
- Mary E. Thompson, Lilia L. Ramirez Ramirez, Vyacheslav Lyubchich, and Yulia R. Gel. Using the bootstrap for statistical inference on random graphs. *Canadian Journal of Statistics*, 44(1):3–24, 2016. ISSN 1708-945X. doi: <https://doi.org/10.1002/cjs.11271>. URL <http://onlinelibrary.wiley.com/doi/abs/10.1002/cjs.11271>. eprint: <https://onlinelibrary.wiley.com/doi/pdf/10.1002/cjs.11271>.
- Craig A. Tracy and Harold Widom. Level-spacing distributions and the Airy kernel. *Communications in Mathematical Physics*, 159(1):151–174, January 1994. ISSN 1432-0916. doi: 10.1007/BF02100489. URL <https://doi.org/10.1007/BF02100489>.
- Joel A Tropp. User-friendly tail bounds for sums of random matrices. *Foundations of computational mathematics*, 12(4):389–434, 2012.
- Y. X. Rachel Wang and Peter J. Bickel. Likelihood-based model selection for stochastic block models. *Annals of Statistics*, 45(2):500–528, April 2017. ISSN 0090-5364, 2168-8966. doi: 10.1214/16-AOS1457. URL <http://projecteuclid.org/euclid.aos/1494921948>. Publisher: Institute of Mathematical Statistics.
- Yi Yu, Tengyao Wang, and Richard J Samworth. A useful variant of the Davis–Kahan theorem for statisticians. *Biometrika*, 102(2):315–323, 2015.
- Yilin Zhang and Karl Rohe. Understanding regularized spectral clustering via graph conductance. In *Proceedings of the 32nd International Conference on Neural Information Processing Systems*, NIPS’18, page 10654–10663, Red Hook, NY, USA, 2018. Curran Associates Inc.

Zhixin Zhou and Arash A. Amini. Optimal bipartite network clustering. *Journal of Machine Learning Research*, 21(40):1–68, 2020. URL <http://jmlr.org/papers/v21/19-299.html>.

Mu Zhu and Ali Ghodsi. Automatic dimensionality selection from the scree plot via the use of profile likelihood. *Computational Statistics & Data Analysis*, 51(2):918–930, November 2006. ISSN 0167-9473. doi: 10.1016/j.csda.2005.09.010. URL <https://www.sciencedirect.com/science/article/pii/S0167947305002343>.